

NEEDLE INSERTION FOR ROBOTIC SURGERY

By

CÉLINE LAPLASSOTTE

A THESIS PRESENTED TO THE GRADUATE SCHOOL
OF THE UNIVERSITY OF FLORIDA IN PARTIAL FULFILLMENT
OF THE REQUIREMENTS FOR THE DEGREE OF
MASTER OF SCIENCE

UNIVERSITY OF FLORIDA

2012

© 2012 Céline Laplassotte

To my family and my friends for their constant encouragement and love.

ACKNOWLEDGMENTS

First of all, I would like to thank my advisor Dr. Dixon for giving me the opportunity to work in his laboratory, Nonlinear Controls and Robotics, for the time he spent with me and for his valuable advices that helped me throughout my project. I shall also thank my research group in which I was particularly well received and for having brought up a lively atmosphere in the daily work.

Furthermore, I am deeply grateful to Dr. Collet, Pr. Tran-Son-Tay and the Atlantis program for having allowed me to take part to this great experience which is studying in a large and well-known university as the University of Florida for one year. And I would like to thank Dr. Bayle for his help and the feedback he gave me on my work.

I would also like to extend my gratitude to my committee member Dr. Carl Crane for the time and help he has provided.

Finally, I would like to thank my family and my friends for their encouragement and all the people I share my work with at the University of Florida.

TABLE OF CONTENTS

	<u>page</u>
ACKNOWLEDGMENTS	4
LIST OF FIGURES	7
ABSTRACT	8
CHAPTER	
1 INTRODUCTION	9
1.1 Motivation and Problem Statement	9
1.2 Literature Review	9
1.3 Outline and Contributions	11
2 NEEDLE INSERTION FORCE DESIGN	13
2.1 Soft Tissue Deformation	13
2.2 Needle Insertion Force Modeling	13
2.2.1 Stiffness Force	15
2.2.2 Friction Force	16
2.2.3 Cutting Force	16
3 ROBOTIC NEEDLE INSERTION INTO VISCOELASTIC TISSUE	18
3.1 Dynamic Model	18
3.2 Control Development	19
3.2.1 Control Objective	19
3.2.2 Closed-Loop Error System	20
3.3 Stability Analysis	24
3.4 Simulation Results	27
4 TELEOPERATED ROBOT FOR NEEDLE INSERTION INTO VISCOELASTIC TISSUE	32
4.1 Dynamic Model	32
4.2 Control Development	33
4.2.1 Control Objective and Model Transformation	33
4.2.2 Closed-Loop Error System	35
4.3 Stability Analysis	38
4.4 Simulation Results	42
5 CONCLUSION	49
5.1 Summary of Results	49
5.2 Recommendations for Future Work	49

REFERENCES	51
BIOGRAPHICAL SKETCH	57

LIST OF FIGURES

<u>Figure</u>	<u>page</u>
2-1 Needle insertion steps	14
3-1 Multilayer neural network for jump function approximation.	21
3-2 Positions for the simulation	28
3-3 Position of the needle tip $x(t)$	29
3-4 Position tracking error $e(t)$	30
3-5 Needle force f_{needle} as a function of time.	30
3-6 Needle force f_{needle} as a function of the needle tip position $x(t)$	31
4-1 Trajectory for master and slave robots for $F_1 = 15 \sin(1.1t)$	44
4-2 Position error between master and slave robot for $F_1 = 15 \sin(1.1t)$	44
4-3 Desired trajectory x_{d2} and position of $q_1 + q_2$ for $F_1 = 15 \sin(1.1t)$	45
4-4 Error between the desired trajectory x_{d2} and $q_1 + q_2$ for $F_1 = 15 \sin(1.1t)$	45
4-5 Trajectory for master and slave robots for $F_1 = 8$	46
4-6 Position error between master and slave robot for $F_1 = 8$	46
4-7 Desired trajectory x_{d2} and position of $q_1 + q_2$ for $F_1 = 8$	47
4-8 Error between the desired trajectory x_{d2} and $q_1 + q_2$ for $F_1 = 8$	47
4-9 Needle force f_{needle} as a function of time for $F_1 = 8$	48
4-10 Needle force f_{needle} as a function of the needle tip position for $F_1 = 8$	48

Abstract of Thesis Presented to the Graduate School
of the University of Florida in Partial Fulfillment of the
Requirements for the Degree of Master of Science

NEEDLE INSERTION FOR ROBOTIC SURGERY

By

Céline Laplassotte

August 2012

Chair: Warren E. Dixon
Major: Mechanical Engineering

Many modern clinical practices involve percutaneous needle insertion. This thesis focuses on modeling and automation aspects related to robotic needle insertion. Medical robotics may offer methods for improving such practices. The first contribution is the development of a controller to ensure that a needle tip tracks a trajectory beginning in a non-contact position and ending within viscoelastic tissue. Through employment of a sliding mode controller and a neural network (NN), the controller guarantees semi-global asymptotic tracking of the desired trajectory. The second contribution is the development of a controller to ensure that a needle tip mounted on a slave robot tracks the trajectory given by the surgeon manipulating the master robot, in the presence of uncertainties in the user and environment forces. The control development leads to semi-global asymptotic tracking of the desired trajectory using a sliding mode controller and a NN. Lyapunov-based stability analysis and simulations are provided to demonstrate the performance of the control designs throughout the thesis.

CHAPTER 1 INTRODUCTION

1.1 Motivation and Problem Statement

Medical robotics has gained popularity over the last decade. Indeed, surgeons all around the world use manipulators to perform surgical procedures. The development of these procedures are motivated by and have improved due to the rapid advancement of minimally invasive procedures [1–4]. Automated and teleoperated systems have the potential to improve the safety and effectiveness of surgeries by enhancing visualization, decreasing bleeding and transfusion rates, and speeding recovery [5].

Many clinical practices involve percutaneous needle insertions. Minimally invasive percutaneous procedures include biopsies [6] and brachytherapy [7] but needle insertion is also used for procedures such as blood sampling [8], neurosurgery [9], and others. In these procedures, one or several needles penetrate into the patient’s body to reach the planned target.

While automated or teleoperated needle insertion systems can lead to various advantages, several issues must be considered including: the lack of visibility of the target, the difficult access to the target, and restricted maneuverability with the tool. For instance, the target may be close to a sensitive organ mandating the need for extra caution and high precision. Targeting error can occur due to imaging limitations, target uncertainties due to physiological or patient motion, human errors due to fatigue or hand tremor, tissue deformation and needle deflection [10]. The efficiency of such a medical treatment is very often linked to the accuracy of the needle insertion and to the control of the insertion force. The desired accuracy depends on the application and usually ranges from millimeter to micro-millimeter. Given such accuracy demands, robotic and teleoperated systems have become increasingly popular tools to assist medical personnel.

1.2 Literature Review

The modeling of needle insertion force into soft tissue can facilitate accurate surgical simulations and robotic technologies applied to percutaneous therapy. The development of such

models has been the topic of many studies [11–17]. Knowledge of forces during needle insertion can help to identify and model different tissue types. Human biological tissues are known to exhibit nonlinear properties and consist of inhomogeneous structures. The Hunt-Crossley model [18] has been confirmed as being suitable for describing the properties of viscoelastic tissues [19], especially when small deformations are involved [20]. Hunt and Crossley showed that it is possible to obtain a behavior that is in better agreement with the physical intuition if the damping coefficient is made dependent on the body's relative penetration. Nevertheless, some studies presume a linear tissue model, especially for computational performance [21]. One of the key issues is that the insertion force varies from one patient to another. For the same tissue, the insertion force can be different depending on the age, the gender, or the body mass of the patient. Even for one patient, the insertion force needed for one tissue can vary, for example, if the tissue is diseased. Moreover, acquiring data from biological tissues and developing appropriate models for application in simulation or robot-assisted surgery is difficult due to tissue deformation, inhomogeneity, nonlinearity, and opacity [22–24]. As a result, it is necessary to design the needle insertion force so that it accounts for the uncertainty in tissue composition.

In medical robotics, a teleoperated system consists of a slave robot which tracks the motion of a master robot commanded by a surgeon, often with the assistance of medical imaging. Many clinical applications benefit from teleoperated systems. Example procedures range from tele-echography [25, 26] to minimally invasive surgery [1, 4, 5, 27, 28]. Teleoperated systems have the ability to reduce the morbidity of clinical procedures by improving the sterile field, decreasing bleeding, and reducing recovery time. However, since the clinician is removed from direct contact with the patient, research efforts have focused on methods to provide improved force reflection, compensate for robotic/tissue uncertainties, and improve the stability and passivity of the system.

The goal of teleoperation systems is to achieve passivity and transparency while maintaining stability. Passivity is related to energy dissipation, a passive system consumes energy and

does not produce energy. To achieve ideal transparency, the slave robot has to exactly reproduce the position trajectory of the master manipulator, and the master robot has to accurately display the environment force to the human. Many bilateral control architectures have been developed to reach these two aims [29–33]. Linear circuit theory [34] and linear robust control theory [35, 36] have been studied in the past. Some works have also been done for nonlinear systems using adaptive control [37–40], however these designs need exact model knowledge. Some previous works highlighted the stability and safe operation of the teleoperator using the passivity concept as in [36, 41–43]. The method proposed in [44] makes the teleoperated system passive using fictitious energy storage. Researches that aim to achieve ideal transparency usually require knowledge about the environment inputs as in [35], or estimate the impedance of the slave robot as in [45]. In [46], an adaptive controller is designed for teleoperated systems with parametric uncertainties in the master and slave robots dynamics. Time delay may also be an issue. In [47], a bilateral teleoperator provides robust stability against constant delay but does not guarantee position tracking.

1.3 Outline and Contributions

Chapter 1 serves as an introduction, that provides motivation, problem statement, literature review, and contributions of the thesis.

Chapter 2 provides a background discussion on soft tissue deformation. This chapter presents also a novel needle insertion force modeling for viscoelastic tissue. The force modeling is designed as the sum of a stiffness force, a friction force, and a cutting force [48]. These three forces are carefully chosen to be as close to the reality as possible. The stiffness force is designed using the Hunt-Crossley model. The friction force is modeled as in [49]. The cutting force is modeled as a constant.

Chapter 3 details the design of an automated controller that ensures semi-global asymptotic tracking of a trajectory for which the needle tip moves from a non-contact position into viscoelastic tissue. The study is based on previous works [50–52], where the objective was to design a controller for a robot interacting with an uncertain Hunt-Crossley viscoelastic

environment and undergoing a non-contact to contact transition but the robot did not go into the viscoelastic environment.

Chapter 4 describes the development of a teleoperated controller to ensure that a needle tip mounted on a slave robot tracks the trajectory given by the surgeon manipulating the master robot, and going from a non-contact position into viscoelastic tissue. The study is based on a previous work [53], where the objective was to design two controllers for a teleoperator system that targets coordination of the master and slave manipulators and passivity of the overall system. As in [53], there is no need to know the user and environment forces in this paper. However, the control development used in [53] is not applicable in the case of a discontinuous needle insertion force. Then, the controller is designed using a sliding mode term and neural network method.

Chapter 5 gives some concluding comments and recommendations for future work.

CHAPTER 2 NEEDLE INSERTION FORCE DESIGN

2.1 Soft Tissue Deformation

Realistic modeling of soft tissue deformation during needle insertion can be used and improved for training and planning to reduce errors between desired and actual placement of the needle tip. This modeling is complex because of the inhomogeneous, nonlinear, anisotropic, elastic and viscous properties of soft tissue. To determine and understand these properties, it is essential to do some measurements on soft tissue [54]. Many ultrasonic methods have been developed for measuring biomechanical properties of soft tissues [55, 56].

Skin and soft tissue exhibit particular properties [57, 58]. The characteristic substances of this kind of tissue are the collagen, elastin and ground substance [59]. At small strains, elastin confers stiffness to the tissue and stores most of the strain energy. The collagen fibers are comparatively inextensible and are usually loose. Soft tissues have the potential to undergo big deformations and still come back to the initial configuration when unloaded. The nonlinear stress-strain relationship results in force not being linearly proportional to displacement [60]. For computational efficiency, however, many researchers assume a simple linear tissue model.

2.2 Needle Insertion Force Modeling

The force modeling used in this study is inspired by [48], where an experimental procedure for acquiring data from ex vivo tissue is given and the needle insertion force is designed as the sum of a stiffness force, a friction force, and a cutting force. In this study, the stiffness force is designed using the nonlinear viscoelastic Hunt-Crossley model. The friction force is modeled as in [49]. This model offers an accurate representation of nonlinear friction effects. The cutting force required to slice through tissue is modeled as a constant depending on the needle size and on the tissue properties [48].

A needle insertion procedure can be divided into three stages. The first stage is a free-space motion and occurs before the needle touches the tissue. The second stage is the needle-tissue viscoelastic interaction and occurs when $x(t) \in \mathbb{R}$, the position of the robot

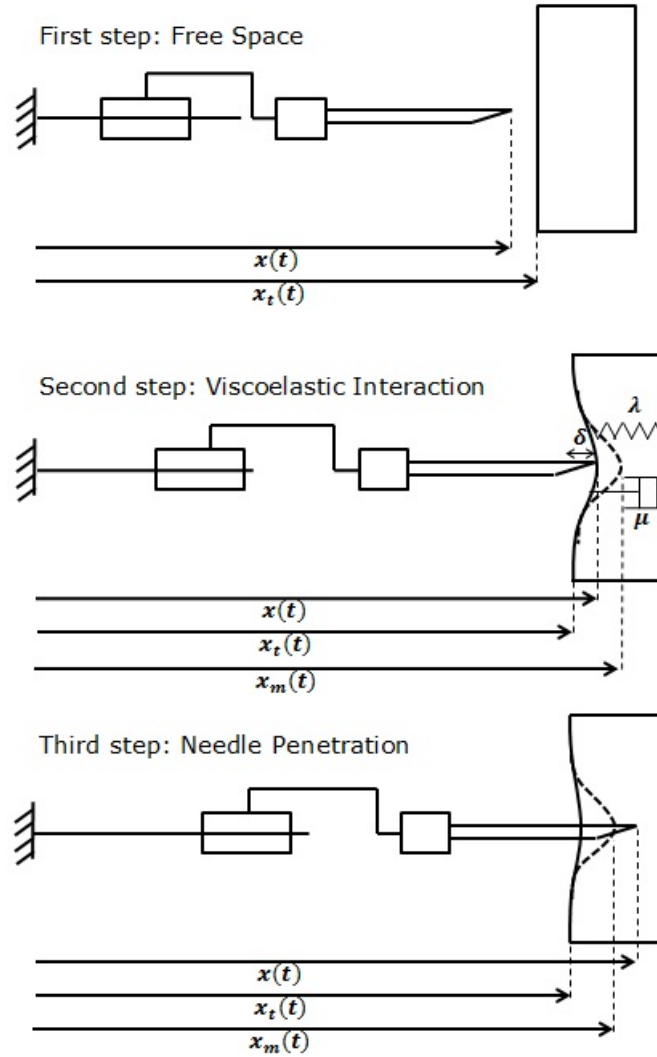


Figure 2-1. Needle insertion steps

end-effector at the needle tip, ranges between $x_t(t) \in \mathbb{R}$, the position of the viscoelastic tissue, and $x_m(t) \in \mathbb{R}$, the position of the maximally deformed tissue surface before puncture. The last stage is the insertion through the tissue, which occurs when $x(t)$ is greater than $x_m(t)$. The dynamics of the tissue depends on forces from surrounding tissue and organs, physiological movements, etc., which result in the evolution of $x_t(t)$ over time. Figure 2-1 illustrates each stage.

The force $f_{needle}(x, \dot{x})$ is discontinuous because of the transition between needle-tissue contact and insertion through the tissue. The needle insertion force can be modeled as [48]

$$f_{needle} \triangleq \Lambda_1 f_{stiffness} + \Lambda_2 f_{friction} + \Lambda_2 f_{cutting}, \quad (2-1)$$

where $\Lambda_1(x, x_t, x_m)$ and $\Lambda_2(x, x_m) \in \mathbb{R}$ are functions which switch at contact and perforation, respectively, defined as

$$\Lambda_1 \triangleq \begin{cases} 1 & x_t \leq x \leq x_m \\ 0 & otherwise \end{cases}, \quad \Lambda_2 \triangleq \begin{cases} 1 & x_m < x \\ 0 & otherwise \end{cases}.$$

2.2.1 Stiffness Force

The stiffness force corresponds to a viscoelastic interaction between the tissue and the needle tip [61]. This interaction occurs before the puncture. The needle compresses the soft tissue until the puncture of the surface. In (2-1), the stiffness force $f_{stiffness}(x, \dot{x}) \in \mathbb{R}$ is described by the Hunt-Crossley model as [18]

$$f_{stiffness} \triangleq \lambda \delta^n + \mu \dot{\delta} \delta^n, \quad (2-2)$$

where $\lambda \in \mathbb{R}$ is the unknown contact stiffness of the viscoelastic mass, $\mu \in \mathbb{R}$ is the unknown damping coefficient, $n \in \mathbb{R}$ is the unknown Hertzian compliance coefficient, and $\delta(t) \in \mathbb{R}$ is the local deformation of the tissue, defined as

$$\delta \triangleq x - x_t. \quad (2-3)$$

The viscoelastic force $f_{stiffness}(x, \dot{x})$ depends on the local deformation of the tissue, while the position of the tissue is the sum of the deformation and the position of the tissue under the pressure of physiological motion or needle tip.

2.2.2 Friction Force

The friction force occurs inside the tissue after the puncture and along the needle shaft. Friction is a natural phenomenon that can be found in many mechanical applications however its modeling is not entirely understood. In (2-1), the friction force $f_{friction}(\dot{x}) \in \mathbb{R}$ is modeled according to [49] as

$$f_{friction} \triangleq \gamma_1 (\tanh(\gamma_2 \dot{x}) - \tanh(\gamma_3 \dot{x})) + \gamma_4 \tanh(\gamma_5 \dot{x}) + \gamma_6 \dot{x}, \quad (2-4)$$

where $\gamma_i \in \mathbb{R}$, for $i = 1, 2, \dots, 6$, are unknown positive constants. The model in (2-4) exhibits the following properties:

1. it is symmetric about the origin,
2. it has a static coefficient of friction, given by $\gamma_1 + \gamma_4$,
3. it includes the Stribeck effect, given by $\tanh(\gamma_2 \dot{x}) - \tanh(\gamma_3 \dot{x})$,
4. it has a viscous dissipation term, given by $\gamma_6 \dot{x}$,
5. it has a Coulombic friction coefficient in the absence of viscous dissipation, given by $\gamma_4 \tanh(\gamma_5 \dot{x})$.

See [49] and [62] for further details.

2.2.3 Cutting Force

Also in (2-1), the cutting force $f_{cutting} \in \mathbb{R}$ represents the force required for the needle to penetrate into the tissue. This force only depends on the needle size and on the tissue properties and is defined as

$$f_{cutting} \triangleq c, \quad (2-5)$$

where $c \in \mathbb{R}$ is a unknown positive constant.

Remark 2.1. In many needle insertion applications, the different parameters of the stiffness force, friction force and cutting force, defined previously in (2-2), (2-4) and (2-5), have to be known. The identification of the needle insertion force can be performed before the operation

using *ex vivo* tests as in [48]. For a medical intervention, *ex vivo* tests can not be done on a patient but these parameters can be determined during the intervention. In [11], an approach for estimating needle force is given but it is not easily applicable for medical procedures because of the need to put markers on the surface. [22] describes an online estimation to determine Hunt-Crossley parameters. For the control analysis developed in the following chapters, these parameters are assumed to be uncertain.

CHAPTER 3 ROBOTIC NEEDLE INSERTION INTO VISCOELASTIC TISSUE

This chapter describes the development of an automated controller to ensure that a needle tip tracks a desired trajectory beginning in a non-contact position and ending within viscoelastic tissue.

3.1 Dynamic Model

The dynamic model for a one-degree-of-freedom translation robot interacting with a viscoelastic environment is

$$M(x)\ddot{x} + h(x) + f_{needle}(x, \dot{x}) = F. \quad (3-1)$$

In (3-1), $x(t)$, $\dot{x}(t)$, $\ddot{x}(t) \in \mathbb{R}$ denote the planar Cartesian position, velocity, and acceleration of the robot end-effector at the needle tip, respectively, $M(x) \in \mathbb{R}$ denotes the uncertain inertia, $h(x) \in \mathbb{R}$ denotes uncertain conservative forces, $f_{needle}(x, \dot{x}) \in \mathbb{R}$, introduced in Chapter 2, denotes the interaction force between the robot at the needle tip and the viscoelastic tissue during the needle insertion procedure, and $F(t) \in \mathbb{R}$ denotes the force control input.

Remark. This study has been developed for a one-degree-of-freedom translation robot but could be extended to the resolution of a redundancy manipulators problem [63].

The following property and assumptions are applied in the control development.

Property 1. The following relationships are valid for all $\xi \in \mathbb{R}$ [64]:

$$\xi \tanh(\xi) \geq \tanh(\xi)^2, \quad (3-2)$$

$$|\tanh(\xi)| \leq 1. \quad (3-3)$$

Assumption 3.1. The robot, tissue, and maximal tissue surface positions, $x(t)$, $x_t(t)$, and $x_m(t)$, introduced in Chapter 2, and the corresponding velocities, $\dot{x}(t)$ and $\dot{x}_t(t)$, are

measurable. Further, it is assumed that the robot trajectory $x(t)$ is bounded due to the geometry of the robot.

Remark 3.1. The position of the maximally deformed tissue surface before puncture $x_m(t)$ can be measured using the technique described in [65].

Assumption 3.2. The local deformation of the viscoelastic material during contact $\delta(x, x_t)$, defined in (2-3), is assumed to be bounded; hence, δ^n can be upper bounded as

$$\delta^n \leq \bar{\delta}^n,$$

where $\bar{\delta}^n \in \mathbb{R}$ is a known positive bounding constant.

Assumption 3.3. The damping constant μ , in (2-2), is assumed to be upper bounded as

$$\mu \leq \bar{\mu},$$

where $\bar{\mu} \in \mathbb{R}$ is a known positive bounding constant.

3.2 Control Development

3.2.1 Control Objective

The control objective is to ensure that the one-degree-of-freedom translation robot tracks a desired position, denoted by $x_d(t) \in \mathbb{R}$, which begins in free space and ends within the viscoelastic tissue. The controller is designed such that the force required to achieve this objective is bounded by an arbitrary small value, which is desired for procedural safety. A position tracking error and a filtered tracking error are designed to quantify the control objective as

$$e \triangleq x_d - x, \tag{3-4}$$

$$r \triangleq \dot{e} + \alpha e, \tag{3-5}$$

where $e(t) \in \mathbb{R}$ represents the position error at the needle tip, $r(t) \in \mathbb{R}$ is a filtered tracking error that facilitates the subsequent control development, and $\alpha \in \mathbb{R}$ is a positive constant control gain.

3.2.2 Closed-Loop Error System

Premultiplying the filtered tracking error $r(t)$ in (3-5) by the robot inertia matrix $M(x)$, taking the time derivative of the resulting expression, and using (3-1) and (3-4) yields the following open-loop robot error system:

$$M\dot{r} = \dot{M}\dot{e} + M\ddot{x}_d + h + f_{needle} - F + \dot{M}\alpha e + M\alpha\dot{e} - \dot{M}r. \quad (3-6)$$

Using the definition of the needle force f_{needle} defined in (2-1), (2-2), (2-4), and (2-5), the expression in (3-6) becomes

$$\begin{aligned} M\dot{r} = & f + \dot{M}\dot{e} + \Lambda_2\gamma_1 (\tanh(\gamma_2\dot{x}) - \tanh(\gamma_3\dot{x})) + \Lambda_2\gamma_4 \tanh(\gamma_5\dot{x}) \\ & + \Lambda_2\gamma_6\dot{x} + \Lambda_2c - F + \dot{M}\alpha e - \dot{M}r, \end{aligned} \quad (3-7)$$

where $f(t) \in \mathbb{R}$ is an auxiliary nonlinear and discontinuous function defined as

$$f \triangleq M\ddot{x}_d + M\alpha\dot{e} + h + \Lambda_1 (\lambda\delta^n + \mu\dot{\delta}\delta^n). \quad (3-8)$$

Based on the universal function approximation property and results from [66] for approximation of jump functions, the discontinuous function $f(t)$ in (3-8) can be approximated by a three-layer (input, hidden, and output) neural network (NN) as

$$f = W_1^T \sigma(V_1^T y) + W_2^T \varphi(V_2^T y) + \varepsilon(y), \quad (3-9)$$

where the NN input $y(t)$ is defined as $y(t) = \begin{bmatrix} 1 & x_t & x & e & r & \delta & \delta\dot{\delta} \end{bmatrix}^T \in \mathbb{R}^7$, $W_1, W_2 \in \mathbb{R}^{(N+1)}$ and $V_1, V_2 \in \mathbb{R}^{7 \times N}$ are ideal NN weights, $N \in \mathbb{R}$ is the number of hidden layer neurons of the NN, $\sigma(V_1^T y) = \sigma \in \mathbb{R}^{N+1}$ is a sigmoid activation function, $\varphi(V_2^T y) = \varphi \in \mathbb{R}^{N+1}$ is

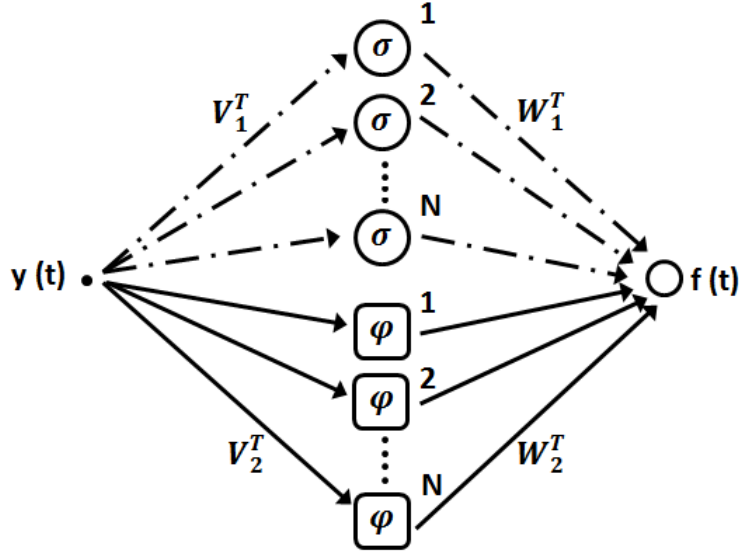


Figure 3-1. Multilayer neural network for jump function approximation.

a sigmoid jump approximation function, and $\varepsilon(y) \in \mathbb{R}$ is the functional reconstruction error of the NN. The weights V_2 are known, given by the designer and depending on the location of the jumps. Figure 3-1 shows the augmented multilayer neural network for jump function approximation. The subsequent stability analysis indicates that, provided some sufficient gain conditions are satisfied, if $y(0)$ is in a compact set, then $y(t)$ remains in a compact set $\forall t$.

Property 2. (Boundedness of the Ideal Weights) The ideal weights are assumed to exist and to be bounded by known positive values so that

$$\|V_i\|_F^2 = \text{tr}(V_i^T V_i) \leq \bar{V}_{iB},$$

$$\|W_i\|_F^2 = \text{tr}(W_i^T W_i) \leq \bar{W}_{iB},$$

where $i = 1, 2$, \bar{V}_{iB} and \bar{W}_{iB} are positive constants, $\|\cdot\|_F$ is the Frobenius norm of a matrix, and $\text{tr}(\cdot)$ is the trace of a matrix.

The estimate for $f(t)$, denoted as $\hat{f}(t) \in \mathbb{R}$, is defined as

$$\hat{f} \triangleq \hat{W}_1^T \sigma(\hat{V}_1^T y) + \hat{W}_2^T \varphi(V_2^T y), \quad (3-10)$$

where $\hat{W}_1(t), \hat{W}_2(t) \in \mathbb{R}^{(N+1)}$ and $\hat{V}_1(t) \in \mathbb{R}^{7 \times N}$ are the estimates of the ideal weights and are generated by integrating the adaptive update laws

$$\begin{aligned}\dot{\hat{W}}_1 &= \text{proj} \left(\Gamma_{w1} \hat{\sigma} r - \Gamma_{w1} \hat{\sigma}' \hat{V}_1^T y r \right), \\ \dot{\hat{V}}_1 &= \text{proj} \left(\Gamma_{v1} y r \hat{W}_1^T \hat{\sigma}' \right), \\ \dot{\hat{W}}_2 &= \text{proj} \left(\Gamma_{w2} \varphi r \right),\end{aligned}\tag{3-11}$$

where $\Gamma_{w1}, \Gamma_{w2} \in \mathbb{R}^{(N+1) \times (N+1)}$ and $\Gamma_{v1} \in \mathbb{R}^{(7 \times 7)}$ are constant, positive definite, diagonal, gain matrices, $\hat{\sigma}' \in \mathbb{R}^{(N+1) \times N}$ denotes the partial derivative of $\hat{\sigma} = \sigma \left(\hat{V}_1^T y \right)$ with respect to its argument, and $\text{proj}(\cdot)$ denotes a smooth projection operator [67, 68]. Based on the fact that $\hat{W}_1(t)$ and $\hat{W}_2(t)$ are bounded by the projection operator, and $\sigma(\cdot)$ and $\varphi(\cdot)$ are bounded activation functions, then $\hat{f}(t)$ can be upper bounded as

$$|\hat{f}| \leq \kappa,\tag{3-12}$$

where $\kappa \in \mathbb{R}$ is a known positive constant.

Based on (3-7) and the subsequent stability analysis, the robot control force input is designed as

$$F = \hat{f} + k_p \tanh(\omega e) + \beta \text{sgn}(r),\tag{3-13}$$

where $k_p, \omega, \beta \in \mathbb{R}$ are positive constant control gains. The smooth saturation function $\tanh(\cdot)$ in (3-13) is used to saturate the terms in the controller to limit the control force during contact and penetration. Using (3-3), (3-12), and the NN projection bounds in [64], the control force in (3-13) can be bounded as

$$|F|_\infty \leq \kappa + k_p + \beta.$$

Using (3-9), (3-10), and (3-13), the expression in (3-7) can be rewritten as

$$\begin{aligned}
M\dot{r} = & W_1^T \sigma + W_2^T \varphi + \varepsilon(y) - \hat{W}_1^T \hat{\sigma} - \hat{W}_2^T \hat{\varphi} - k_p \tanh(\omega e) \\
& - \beta \operatorname{sgn}(r) + \dot{M}e + \Lambda_2 \gamma_1 (\tanh(\gamma_2 \dot{x}) - \tanh(\gamma_3 \dot{x})) \\
& + \Lambda_2 \gamma_4 \tanh(\gamma_5 \dot{x}) + \Lambda_2 \gamma_6 \dot{x} + \Lambda_2 c + \dot{M} \alpha e - \dot{M} r.
\end{aligned} \tag{3-14}$$

Using the Taylor series expansion [66], the term $\tilde{\sigma} = \sigma - \hat{\sigma}$ can be written as

$$\tilde{\sigma} = \hat{\sigma}' \tilde{V}_1^T y + O\left(\tilde{V}_1^T y\right)^2,$$

where $\tilde{W}_1(t) \in \mathbb{R}^{(N+1)}$ and $\tilde{V}_1(t) \in \mathbb{R}^{7 \times N}$ are estimate errors of the ideal weights and are defined as

$$\tilde{W}_1 = W_1 - \hat{W}_1, \quad \tilde{V}_1 = V_1 - \hat{V}_1, \quad \tilde{W}_2 = W_2 - \hat{W}_2.$$

After some algebraic manipulations, the expression in (3-14) can be expressed as

$$\begin{aligned}
M\dot{r} = & \tilde{W}_1^T \hat{\sigma} + \hat{W}_1^T \hat{\sigma}' \tilde{V}_1^T y - \tilde{W}_1^T \hat{\sigma}' \hat{V}_1^T y + \tilde{W}_2^T \varphi + \Delta - k_p \tanh(\omega e) \\
& - \beta \operatorname{sgn}(r) - \frac{1}{2} \dot{M} r - k r - e,
\end{aligned} \tag{3-15}$$

where $k \in \mathbb{R}$ is a positive constant, the state vector $z \in \mathbb{R}^2$ is defined as $z(e, r) \triangleq \begin{bmatrix} e(t) & r(t) \end{bmatrix}^T$, and $\Delta(z) \in \mathbb{R}$ is defined as

$$\begin{aligned}
\Delta = & \tilde{W}_1^T \hat{\sigma}' \tilde{V}_1^T y + W_1^T O\left(\tilde{V}_1^T y\right)^2 + \varepsilon(y) + \Lambda_2 \gamma_1 (\tanh(\gamma_2 \dot{x}) - \tanh(\gamma_3 \dot{x})) \\
& + \Lambda_2 \gamma_6 \dot{x} + \dot{M}e - \frac{1}{2} \dot{M} r + \Lambda_2 \gamma_4 \tanh(\gamma_5 \dot{x}) + \Lambda_2 c + \dot{M} \alpha e + k r + e.
\end{aligned} \tag{3-16}$$

Using (3-11), (3-16), and [69], an upper bound for $\Delta(z)$ can be determined as

$$|\Delta| \leq \zeta + \rho(\|z\|) \|z\|, \tag{3-17}$$

where $\rho(\cdot) \in \mathbb{R}$ is a positive, globally invertible function, and $\zeta \in \mathbb{R}$ is a known positive constant.

3.3 Stability Analysis

Theorem 3.1. *The controller given in (3–13) ensures semi-global tracking in the sense that*

$$e(t) \rightarrow 0 \quad \text{as } t \rightarrow \infty,$$

provided control gains are selected sufficiently large (see the subsequent stability analysis).

Proof. Let $\mathcal{D} \subset \mathbb{R}^3$ be a domain containing $v(t) = 0$, where $v(t) \in \mathbb{R}^3$ is defined as

$$v(t) \triangleq \begin{bmatrix} z^T(t) & \sqrt{Q(t)} \end{bmatrix}^T, \quad (3-18)$$

and the auxiliary function $Q(t) \in \mathbb{R}$ is defined as

$$Q(t) \triangleq \frac{1}{2} \text{tr} \left(\tilde{V}_1^T \Gamma_{v_1}^{-1} \tilde{V}_1 \right) + \frac{1}{2} \text{tr} \left(\tilde{W}_1^T \Gamma_{w_1}^{-1} \tilde{W}_1 \right) + \frac{1}{2} \text{tr} \left(\tilde{W}_2^T \Gamma_{w_2}^{-1} \tilde{W}_2 \right).$$

Since Γ_{v_1} , Γ_{w_1} and Γ_{w_2} are constant, symmetric, and positive definite matrices, it is straightforward that $Q(t) \geq 0$.

Let $V(v, t) : \mathcal{D} \times [0, \infty) \rightarrow \mathbb{R}$ be a Lipschitz continuous regular positive definite function defined as

$$V \triangleq \frac{1}{2} M r^2 + \frac{1}{2} e^2 + \frac{k_p}{\omega} \ln(\cosh(\omega e)) + Q, \quad (3-19)$$

which satisfies the following inequalities:

$$U_1(v) \leq V(v, t) \leq U_2(v),$$

where the continuous positive definite functions $U_1(v)$, $U_2(v) \in \mathbb{R}$ are defined as

$$U_1(v) \triangleq \eta_1 \|v\|^2, \quad U_2(v) \triangleq \eta_2 \|v\|^2, \quad (3-20)$$

where $\eta_1, \eta_2 \in \mathbb{R}$ are known positive constants.

The differential equations of the closed loop dynamics given in (3–15) are continuous except in sets $\{v | x = x_t\}$ and $\{v | r = 0\}$. Using Filippov's differential inclusion [70], the existence of solutions can be established for $\dot{v} = f(v)$, where $f(v) \in \mathbb{R}^3$ denotes the right-hand side of the closed-loop error signals. Under Filippov's framework, a generalized Lyapunov stability theory can be used to establish strong stability of the closed-loop error system. The generalized time derivative of (3–19) exists almost everywhere (a.e.), and $\dot{V}(v) \in^{a.e.} \check{V}(v)$ where

$$\check{V} = \bigcap_{\xi \in \partial V(v)} K \left[\begin{array}{c} \dot{r} \\ \dot{e} \\ \frac{1}{2}Q^{-\frac{1}{2}}\dot{Q} \end{array} \right]^T,$$

where ∂V is the generalized gradient of $V(v)$ [71], $K[\cdot]$ is defined as [72, 73]

$$K[f] \triangleq \bigcap_{\delta > 0} \bigcap_{\mu \Upsilon = 0} \bar{co}f(B(x, \delta) - \Upsilon),$$

where $\bigcap_{\mu \Upsilon = 0}$ denotes the intersection of all sets Υ of Lebesgue measure zero, \bar{co} denotes convex closure, and $B(x, \delta) = \{u \in \mathbb{R}^3 | \|u - v\| < \delta\}$. Since $V(v)$ is a Lipschitz continuous regular function

$$\begin{aligned} \dot{V} &= \nabla V^T K \left[\begin{array}{c} \dot{r} \\ \dot{e} \\ \frac{1}{2}Q^{-\frac{1}{2}}\dot{Q} \end{array} \right]^T \\ &\subset \left[\begin{array}{ccc} Mr & e & \frac{k_p}{\omega} \tanh(\omega e) \end{array} \right]^T K \left[\begin{array}{c} \dot{r} \\ \dot{e} \\ \frac{1}{2}Q^{-\frac{1}{2}}\dot{Q} \end{array} \right]^T. \end{aligned} \quad (3-21)$$

Using (3–5), (3–11), and (3–15), the expression in (3–21) becomes

$$\dot{V} \subset r\Delta - \beta|r| - kr^2 - \alpha e^2 - \tanh(\omega e) k_p \alpha e. \quad (3-22)$$

Using (3–2) and (3–17), the expression in (3–22) can be upper bounded as

$$\dot{V} \stackrel{a.e.}{\leq} \rho(\|z\|) |r| \|z\| - (\beta - \zeta) |r| - kr^2 - \alpha e^2 - \frac{k_p \alpha}{\omega} |\tanh(\omega e)|^2. \quad (3-23)$$

Let the control gain k in (3–15) be defined as

$$k \triangleq k_1 + k_2, \quad (3-24)$$

where $k_1, k_2 \in \mathbb{R}$ are known positive constants. Using (3-24) and the gain condition

$$\beta > \zeta,$$

the expression in (3-23) can be upper bounded as

$$\dot{V} \stackrel{a.e.}{\leq} - \left(k_1 r^2 - \rho(\|z\|) r \|z\| \right) - k_2 r^2 - \alpha e^2. \quad (3-25)$$

Completing the squares on the term in parentheses in (3-25) yields

$$\dot{V} \stackrel{a.e.}{\leq} \frac{\rho(\|z\|)^2}{4k_1} \|z\|^2 - k_2 r^2 - \alpha e^2. \quad (3-26)$$

The expression in (3-26) can be further upper bounded as

$$\dot{V} \stackrel{a.e.}{\leq} -\lambda \|z\|^2 + \frac{\rho(\|z\|)^2}{4k_1} \|z\|^2, \quad (3-27)$$

where $\lambda = \min\{k_2, \alpha\}$ is a known positive constant. Finally, given the gain condition

$$\lambda > \frac{\rho(\|z\|)^2}{4k_1},$$

the expression in (3-27) becomes

$$\dot{V} \stackrel{a.e.}{\leq} -U(v), \quad (3-28)$$

where $U(v) = \vartheta \|z\|^2$, for some positive constant $\vartheta \in \mathbb{R}$, is a continuous positive semi-definite function such that

$$\mathcal{D} \triangleq \left\{ v \in \mathbb{R}^3 \mid \|v\| \leq \rho^{-1} \left(2\sqrt{\lambda k_1} \right) \right\}.$$

The expressions in (3-19) and (3-28) can be used to show that $V(v, t) \in \mathcal{L}_\infty$; hence, $e(t), r(t)$, and $Q(t) \in \mathcal{L}_\infty$ in \mathcal{D} . Given that $e(t), r(t) \in \mathcal{L}_\infty$ in \mathcal{D} , it can be proven that $\dot{e}(t) \in \mathcal{L}_\infty$ in \mathcal{D} from (3-5). Since $e(t), r(t) \in \mathcal{L}_\infty$ in \mathcal{D} , the assumption that $x_d(t), \dot{x}_d(t)$

exist and are bounded can be used to conclude that $x(t), \dot{x}(t) \in \mathcal{L}_\infty$ in \mathcal{D} . Similarly, it can be shown that $\dot{r}(t) \in \mathcal{L}_\infty$ in \mathcal{D} . Since $\dot{e}(t), \dot{r}(t) \in \mathcal{L}_\infty$ in \mathcal{D} , the definitions for $U(v)$ and $z(t)$ can be used to prove that $U(v)$ is uniformly continuous in \mathcal{D} .

Let $\mathcal{S} \subset \mathcal{D}$ denotes a set defined as follows:

$$\mathcal{S} \triangleq \left\{ v(t) \in \mathcal{D} \mid U_2(v(t)) < \eta_1 \left(\rho^{-1} \left(2\sqrt{\lambda k_1} \right) \right)^2 \right\}.$$

[74] can now be invoked to state that

$$\|z(t)\|^2 \rightarrow 0 \quad \text{as } t \rightarrow \infty \quad \forall v(0) \in \mathcal{S}. \quad (3-29)$$

Based on the definition of $v(t)$ in (3-18), (3-29) can be used to show that

$$|e(t)| \rightarrow 0 \quad \text{as } t \rightarrow \infty \quad \forall v(0) \in \mathcal{S}.$$

□

3.4 Simulation Results

The developed controller is simulated for a system whose dynamic model is given by

$$m\ddot{x} + b\dot{x} + f_{needle}(x, \dot{x}) = F,$$

where $F(t)$ and $f_{needle}(x, \dot{x})$ are introduced in 3-1, $m = 0.152 \text{ kg}$, $b = 1.426 \text{ N} \cdot \text{s} \cdot \text{m}^{-1}$, which correspond to the needle insertion robot described in [75]. The different position and parameter values are chosen to agree with a direct insertion into the liver. The initial needle tip position is supposed to be at $x = 0$ for $t = 0$. For sake of simplicity, it is assumed that the tissue position x_t does not depend on time and its value is fixed to $x_t = 20 \text{ mm}$. The position of the maximally deformed tissue surface before puncture is chosen as $x_m = 36 \text{ mm}$, which means that the needle progresses 16 mm while in contact with the liver before the puncture occurs. The desired position is chosen as $x_d = 60 \text{ mm}$, which correspond to 40 mm into the liver. Figure 3-2 shows the choice of the different positions for that simulation. The

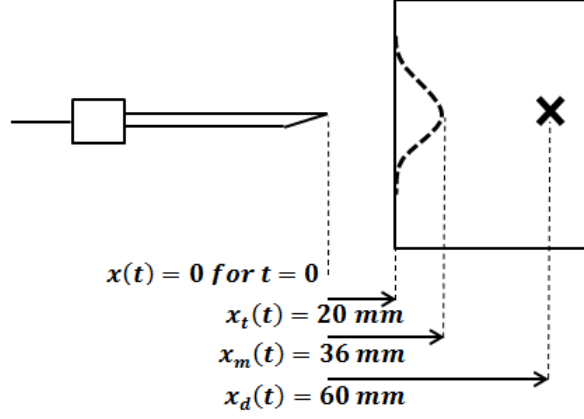


Figure 3-2. Positions for the simulation

parameters for $f_{stiffness}(x, \dot{x})$, $f_{friction}(\dot{x})$, and $f_{cutting}$, introduced in Chapter 2, are chosen as

$$\lambda = 0.2 \text{ N} \cdot \text{m}^{-1}, \quad \mu = 5.5 \text{ N} \cdot \text{s} \cdot \text{m}^{-2}, \quad n = 1.5, \quad \gamma_1 = \gamma_4 = 0.1 \text{ N}, \quad (3-30)$$

$$\gamma_2 = \gamma_3 = \gamma_5 = 0.2 \text{ s} \cdot \text{m}^{-1}, \quad \gamma_6 = 0.5 \text{ N} \cdot \text{s} \cdot \text{m}^{-1}, \quad c = 0.94 \text{ N}.$$

The parameters in (3-30) are selected using results from experiments on liver [48, 65]. The controller gains introduced in (3-13) and the control gain α introduced in (3-5) are selected as

$$k_p = 5, \quad \omega = 1, \quad \beta = 2, \quad \alpha = 10.$$

The number of hidden layer neurons for the NN is chosen as $N = 15$, and the NN weight updation gains are selected as

$$\Gamma_{w1} = \Gamma_{w2} = 5I_{16}, \quad \Gamma_{v1} = 5I_5,$$

where $I_p \in \mathbb{R}^{p \times p}$ denotes the identity matrix.

Figure 3-3 shows the position of the needle tip $x(t)$, which asymptotically approaches the desired position $x_d = 60 \text{ mm}$. Then, the error goes to zero as time goes to infinity as shown in Figure 3-4. During the first stage, between 0 and 20 mm or between 0 and 54 ms, the force between the needle and the tissue is equal to zero because the needle does not touch the tissue yet as it can be seen on Figures 3-5 and 3-6. Then, between 20 mm and the maximally

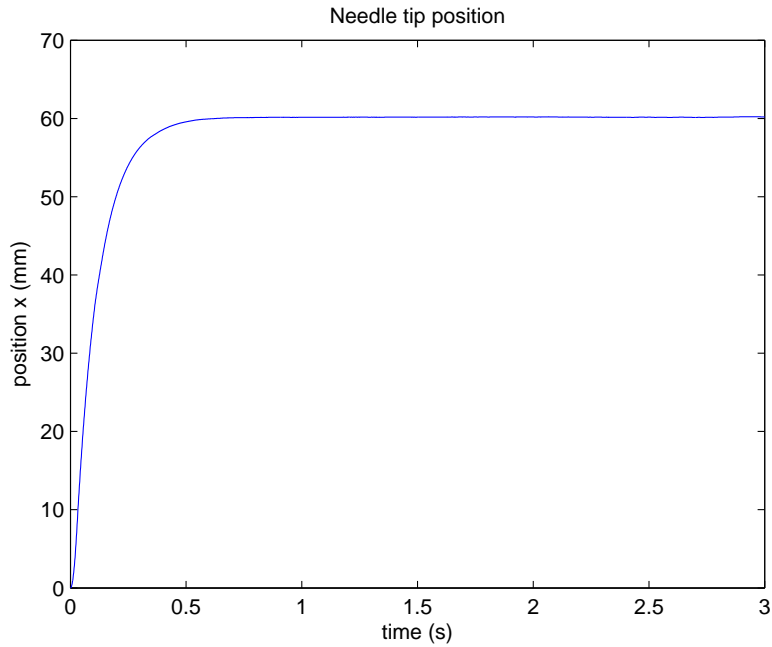


Figure 3-3. Position of the needle tip $x(t)$.

deformed tissue at 36 mm , the needle force increases, as the needle contacts the tissue; the needle force is then equal to the Hunt-Crossley force. The maximum force (3.6 N) is followed by a sudden drop in force as the needle punctures the tissue and now only needs to overcome the friction and cutting forces, which are smaller than the tissue stiffness force. The last stage is the insertion through the tissue to reach the target.

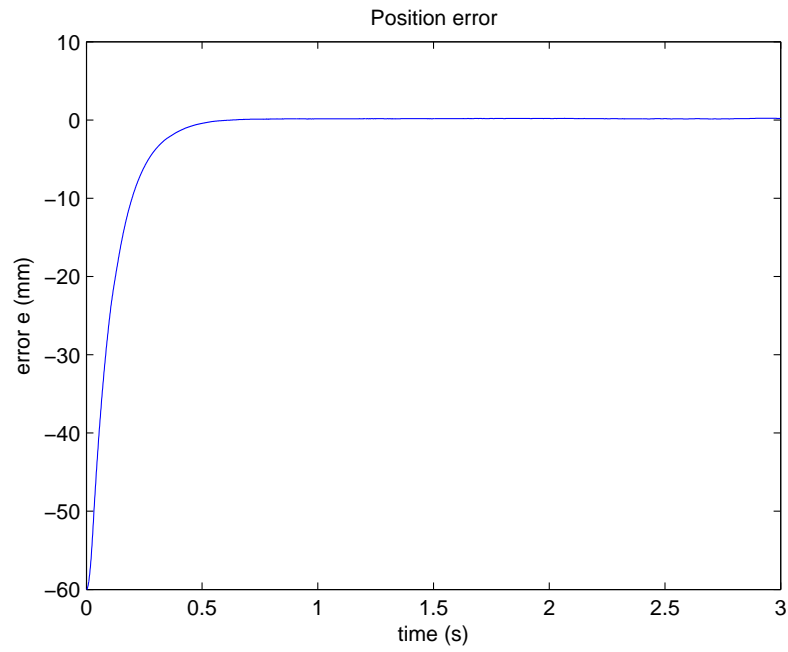


Figure 3-4. Position tracking error $e(t)$.

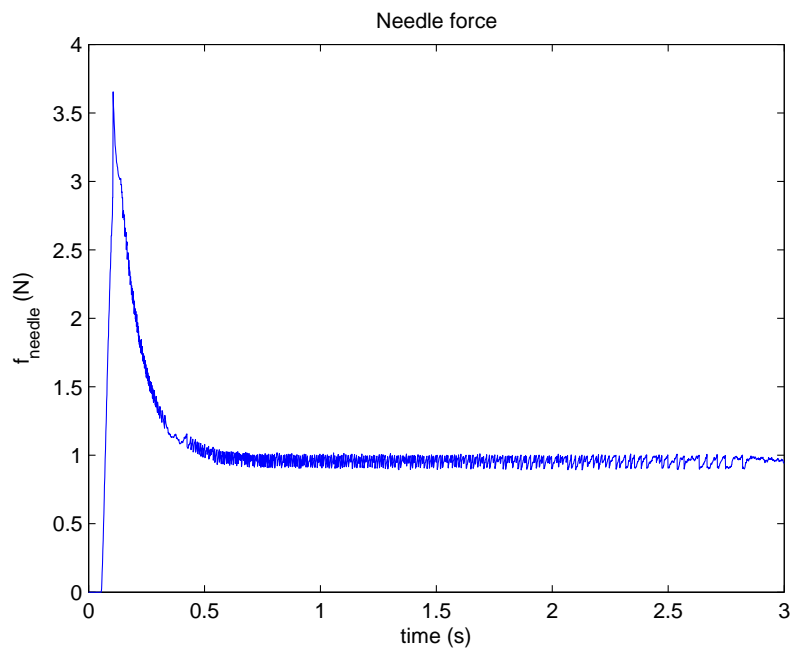


Figure 3-5. Needle force f_{needle} as a function of time.

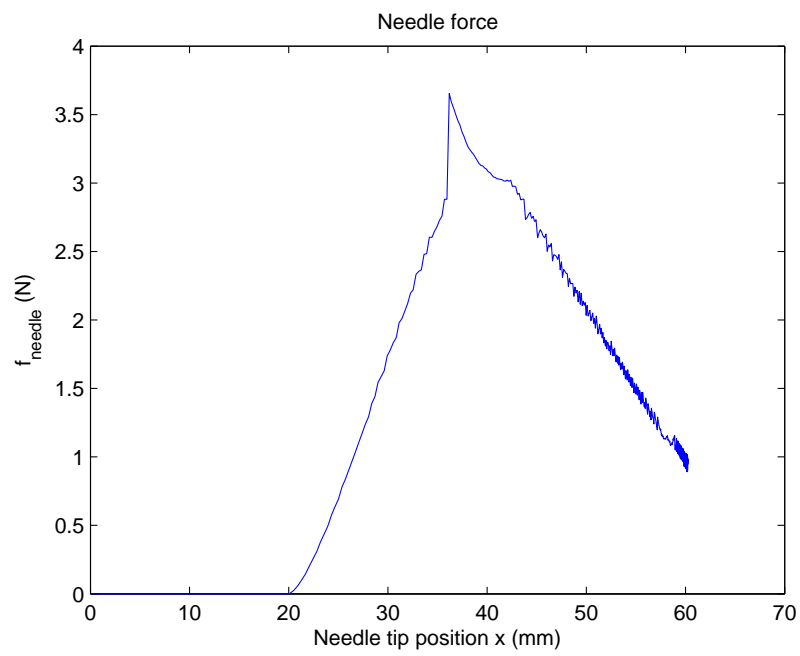


Figure 3-6. Needle force f_{needle} as a function of the needle tip position $x(t)$.

CHAPTER 4
TELEOPERATED ROBOT FOR NEEDLE INSERTION INTO VISCOELASTIC TISSUE

This chapter describes the development of a controller to ensure that a needle tip mounted on a slave robot tracks the trajectory given by the surgeon manipulating the master robot. The trajectory moves from a non-contact position into viscoelastic tissue.

4.1 Dynamic Model

The dynamic model for a one-degree-of-freedom translation master and a one-degree-of-freedom translation slave robot is described by

$$\gamma (T_1 + F_1) = \gamma (M_1 (q_1) \ddot{q}_1 + h_1 (q_1)), \quad (4-1)$$

$$T_2 - F_2 = M_2 (q_2) \ddot{q}_2 + h_2 (q_2). \quad (4-2)$$

In (4-1) and (4-2), $\gamma \in \mathbb{R}$ denotes a positive adjustable power scaling term, $q_i (t)$, $\dot{q}_i (t)$, $\ddot{q}_i (t) \in \mathbb{R}$ denote the robot end-effector position, velocity, and acceleration, respectively, $\forall i = 1, 2$ where $i = 1$ denotes the master manipulator and $i = 2$ denotes the slave manipulator, $M_i (q_i) \in \mathbb{R}$ denotes the inertia, $h_i (q_i) \in \mathbb{R}$ denotes conservative forces, $T_i (t) \in \mathbb{R}$ denotes the force control input, $F_1 (t) \in \mathbb{R}$ denotes the user input force, and $F_2 (t) \in \mathbb{R}$ denotes the force input from the environment, i.e., the interaction force between the robot and the tissue during the needle insertion. The force $F_2 (t)$ is discontinuous because of the transition between needle-tissue contact and insertion through the tissue.

Assumption 4.1. The position $q_i (t)$ and the velocity $\dot{q}_i (t)$ are measurable.

Assumption 4.2. The user force $F_1 (t)$ and the environment force $F_2 (t)$ are bounded.

Assumption 4.3. The dynamic models of the two robots are known.

4.2 Control Development

4.2.1 Control Objective and Model Transformation

The first control objective is to ensure that the slave robot tracks the master robot position, which goes from a free-space position into a viscoelastic tissue, in the following sense:

$$q_2(t) \rightarrow q_1(t) \text{ as } t \rightarrow \infty.$$

Energetic passivity is important to ensure the robot interacts with the tissue in a stable and safe manner. Then, the other objective is to ensure that the system remains passive with respect to the scaled user and environmental power in the sense that [76]

$$\int_{t_0}^t (\gamma \dot{q}_1(\tau) F_1(\tau) - \dot{q}_2 F_2(\tau)) d\tau \geq -c, \quad (4-3)$$

where $c \in \mathbb{R}$ is a positive constant which depends on the initial condition, and γ was introduced in (4-1). The equation in (4-3) means that the energy produces by the slave robot can not be bigger than the sum of the energy from the master robot and the initial energy in the system. An auxiliary control objective is employed to ensure the passivity objective, in the sense that [41]

$$q_1(t) + q_2(t) \rightarrow x_{d2}(t) \text{ as } t \rightarrow \infty, \quad (4-4)$$

where $x_d(t) = \begin{bmatrix} x_{d1}(t) & x_{d2}(t) \end{bmatrix}^T \in \mathbb{R}^2$ is a desired bounded trajectory.

To facilitate the subsequent development, a globally invertible transformation is defined that encodes both the coordination and the passivity objectives, i.e.,

$$x \triangleq Sq + \begin{bmatrix} x_{d1} \\ 0 \end{bmatrix}, \quad (4-5)$$

where $x(t) \triangleq \begin{bmatrix} x_1(t) & x_2(t) \end{bmatrix}^T \in \mathbb{R}^2$, $q(t) \triangleq \begin{bmatrix} q_1(t) & q_2(t) \end{bmatrix}^T \in \mathbb{R}^2$, and $S \in \mathbb{R}^{2 \times 2}$ is defined as follows:

$$S \triangleq \begin{bmatrix} 1 & -1 \\ 1 & 1 \end{bmatrix}, \quad S^{-1} \triangleq \frac{1}{2} \begin{bmatrix} 1 & 1 \\ -1 & 1 \end{bmatrix}. \quad (4-6)$$

Based on (4-5), the dynamic model given in (4-1) and (4-2) can be expressed as

$$\bar{M}(x) \ddot{x} - \bar{M}(x) \begin{bmatrix} \ddot{x}_{d1} \\ 0 \end{bmatrix} + \bar{h}(x) = \bar{T}(t) + \bar{F}(t), \quad (4-7)$$

where

$$\bar{M}(x) \triangleq S^{-T} \begin{bmatrix} \gamma M_1 & 0 \\ 0 & M_2 \end{bmatrix} S^{-1} \in \mathbb{R}^{2 \times 2}, \quad (4-8)$$

$$\bar{h}(x) \triangleq S^{-T} \begin{bmatrix} \gamma h_1 \\ h_2 \end{bmatrix} \in \mathbb{R}^2,$$

$$\bar{T}(t) \triangleq S^{-T} \begin{bmatrix} \gamma T_1 \\ T_2 \end{bmatrix} \in \mathbb{R}^2,$$

$$\bar{F}(t) \triangleq \begin{bmatrix} \bar{F}_1 \\ \bar{F}_2 \end{bmatrix} = S^{-T} \begin{bmatrix} \gamma F_1 \\ -F_2 \end{bmatrix} \in \mathbb{R}^2. \quad (4-9)$$

Property 3. The subsequent development is based on the property that $\bar{M}(x)$, defined in (4-8), is a positive definite and symmetric matrix in the sense that

$$\bar{m}_1 \|\xi\|^2 \leq \xi^T \bar{M}(x) \xi \leq \bar{m}_2 \|\xi\|^2, \quad (4-10)$$

where $\xi \in \mathbb{R}^2$, and $\bar{m}_1, \bar{m}_2 \in \mathbb{R}$ are positive constants.

A position tracking error $e_1(t) \in \mathbb{R}^2$ and a filtered tracking error $e_2(t) \in \mathbb{R}^2$ are designed to quantify the control objective as

$$e_1 \triangleq x - x_d, \quad (4-11)$$

$$e_2 \triangleq \dot{e}_1 + \alpha_1 e_1, \quad (4-12)$$

where $\alpha_1 \in \mathbb{R}$ is a positive constant control gain, and $x_d(t) \in \mathbb{R}^2$ is introduced in (4-4).

Based on the definition of $x(t)$ in (4-5) and $e_1(t)$ in (4-11), it is clear that if $\|e_1\| \rightarrow 0$ as

$t \rightarrow \infty$ then $q_2(t) \rightarrow q_1(t)$ and $q_1(t) + q_2(t) \rightarrow x_{d2}(t)$ as $t \rightarrow \infty$. To ensure that the system remains passive as defined in (4-4), the desired trajectory $x_d(t)$ is generated by the following expression

$$\bar{M}\ddot{x}_d + B_T\dot{x}_d + K_Tx_d + \frac{1}{2}\bar{M}\dot{x}_d = \hat{F}, \quad (4-13)$$

where $B_T, K_T \in \mathbb{R}$ represent positive constants, $\bar{M} \in \mathbb{R}^{2 \times 2}$ is introduced in (4-8), and $\hat{F} \in \mathbb{R}^2$ is a subsequently designed force estimator.

4.2.2 Closed-Loop Error System

Premultiplying the second time derivative of the tracking error $e_1(t)$ in (4-11) by the robot inertia matrix $\bar{M}(x)$, and using the system dynamics (4-7) and the desired trajectory dynamics (4-13), the open-loop robot error system can be written as

$$\bar{M}\ddot{e}_1 = \bar{T} + \bar{F} + \bar{M} \begin{bmatrix} \ddot{x}_{d1} \\ 0 \end{bmatrix} - \bar{h} - \hat{F} + B_T\dot{x}_d + K_Tx_d + \frac{1}{2}\bar{M}\dot{x}_d. \quad (4-14)$$

Based on the assumption of exact model knowledge of the robot dynamics and the subsequent stability analysis, the robot control input $\bar{T}(t)$ is designed as

$$\begin{aligned} \bar{T} \triangleq & -\bar{M} \begin{bmatrix} \ddot{x}_{d1} \\ 0 \end{bmatrix} + \bar{h} - B_T\dot{x}_d - K_Tx_d - \frac{1}{2}\bar{M}\dot{x}_d - \bar{M}\alpha_1e_1 \\ & - \beta \text{sgn}(e_2) - \frac{1}{2}e_2^T \dot{\bar{M}}e_2, \end{aligned} \quad (4-15)$$

where $\beta \in \mathbb{R}$ is a positive constant control gain. Using (4-15), (4-14) can be written as

$$\bar{M}\ddot{e}_1 = \bar{F} - \hat{F} - \bar{M}\alpha_1e_1 - \beta \text{sgn}(e_2) - \frac{1}{2}e_2^T \dot{\bar{M}}e_2. \quad (4-16)$$

Using (4-16) and the time derivative of the filtered tracking error $e_2(t)$, (4-12) becomes

$$\bar{M}\dot{e}_2 = \bar{F} - \hat{F} - \beta \text{sgn}(e_2) - \frac{1}{2}e_2^T \dot{\bar{M}}e_2. \quad (4-17)$$

Based on the universal function approximation property and results from [66] for approximation of jump functions, the discontinuous force $\bar{F}(t)$, defined in (4–9), can be approximated by a three-layer (input, hidden, and output) neural network (NN) as

$$\bar{F} = W_1^T \sigma(V_1^T y) + W_2^T \varphi(V_2^T y) + \varepsilon(y), \quad (4-18)$$

where the NN input $y(t)$ is defined as $y(t) = \begin{bmatrix} 1 & x^T & e_1^T & e_2^T \end{bmatrix}^T \in \mathbb{R}^7$, $W_1, W_2 \in \mathbb{R}^{(N+1) \times 2}$ and $V_1, V_2 \in \mathbb{R}^{7 \times N}$ are ideal NN weights, $N \in \mathbb{R}$ is the number of hidden layer neurons of the NN, $\sigma(V_1^T y) = \sigma \in \mathbb{R}^{N+1}$ is a sigmoid activation function, $\varphi(V_2^T y) = \varphi \in \mathbb{R}^{N+1}$ is a sigmoid jump approximation function, and $\varepsilon(y) \in \mathbb{R}^2$ is the functional reconstruction error of the NN.

The weights V_2 are known, given by the designer and depend on the location of the jumps. The subsequent stability analysis indicates that, provided some sufficient gain conditions are satisfied, if $y(0)$ is in a compact set, then $y(t)$ remains in a compact set $\forall t$.

Property 4. (Boundedness of the Ideal Weights) The ideal weights are assumed to exist and to be bounded by known positive values so that

$$\begin{aligned} \|V_i\|_F^2 &= tr(V_i^T V_i) \leq \bar{V}_{iB}, \\ \|W_i\|_F^2 &= tr(W_i^T W_i) \leq \bar{W}_{iB}, \end{aligned}$$

where \bar{V}_{iB} and \bar{W}_{iB} are positive constants for $i = 1, 2$, $\|\cdot\|_F$ is the Frobenius norm of a matrix, and $tr(\cdot)$ is the trace of a matrix.

The estimate for $\bar{F}(t)$, denoted as $\hat{F}(t) \in \mathbb{R}^2$, is defined as

$$\hat{F} \triangleq \hat{W}_1^T \sigma(\hat{V}_1^T y) + \hat{W}_2^T \varphi(V_2^T y), \quad (4-19)$$

where $\hat{W}_1(t), \hat{W}_2(t) \in \mathbb{R}^{(N+1) \times 2}$ and $\hat{V}_1(t) \in \mathbb{R}^{7 \times N}$ are the estimates of the ideal weights and are generated by integrating the adaptive update laws

$$\begin{aligned}
\dot{\hat{W}}_1 &\triangleq \text{proj} \left(\Gamma_{w1} \hat{\sigma} e_2^T - \Gamma_{w1} \hat{\sigma}' \hat{V}_1^T y e_2^T \right), \\
\dot{\hat{V}}_1 &\triangleq \text{proj} \left(\Gamma_{v1} y e_2^T \hat{W}_1^T \hat{\sigma}' \right), \\
\dot{\hat{W}}_2 &\triangleq \text{proj} \left(\Gamma_{w2} \varphi e_2^T \right),
\end{aligned} \tag{4-20}$$

where $\Gamma_{w1}, \Gamma_{w2} \in \mathbb{R}^{(N+1) \times (N+1)}$ and $\Gamma_{v1} \in \mathbb{R}^{(7 \times 7)}$ are constant, positive definite, diagonal, gain matrices; $\hat{\sigma}' \in \mathbb{R}^{(N+1) \times N}$ denotes the partial derivative of $\hat{\sigma} = \sigma(\hat{V}_1^T y)$ with respect to its argument, and $\text{proj}(\cdot)$ denotes a smooth projection operator [67, 68]. Based on the fact that $\hat{W}_1(t)$ and $\hat{W}_2(t)$ are bounded by the projection operator, and $\sigma(\cdot)$ and $\varphi(\cdot)$ are bounded activation functions, then $\hat{F}(t)$ can be upper bounded as

$$\|\hat{F}\| \leq \kappa, \tag{4-21}$$

where $\kappa \in \mathbb{R}$ is a known positive constant. Using (4-15), (4-18), and (4-19), the expression in (4-17) can be rewritten as

$$\bar{M} \dot{e}_2 = W_1^T \sigma + W_2^T \varphi + \varepsilon(y) - \hat{W}_1^T \hat{\sigma} - \hat{W}_2^T \varphi - \beta \text{sgn}(e_2) - \frac{1}{2} e_2^T \dot{M} e_2. \tag{4-22}$$

The estimate errors of the ideal weights $\tilde{W}_1(t) \in \mathbb{R}^{(N+1) \times 2}$, $\tilde{V}_1(t) \in \mathbb{R}^{7 \times N}$, and $\tilde{W}_2 \in \mathbb{R}^{(N+1) \times 2}$ are defined as

$$\tilde{W}_1 = W_1 - \hat{W}_1, \quad \tilde{V}_1 = V_1 - \hat{V}_1, \quad \tilde{W}_2 = W_2 - \hat{W}_2.$$

Using the Taylor series expansion [66], the estimate error of the activation $\tilde{\sigma} \in \mathbb{R}^{N+1}$, defined as $\tilde{\sigma} = \sigma - \hat{\sigma}$, can be written as

$$\tilde{\sigma} = \hat{\sigma}' \tilde{V}_1^T y + O\left(\tilde{V}_1^T y\right)^2. \tag{4-23}$$

Using (4-23) and the expression in (4-22), the closed-loop error system can be written as

$$\begin{aligned} \bar{M}\dot{e}_2 &= \tilde{W}_1^T \hat{\sigma} + \hat{W}_1^T \hat{\sigma}' \tilde{V}_1^T y - \tilde{W}_1^T \hat{\sigma}' \hat{V}_1^T y + \tilde{W}_2^T \varphi + \Delta - \beta \text{sgn}(e_2) \\ &\quad - \frac{1}{2} e_2^T \dot{M} e_2 - k e_2 - e_1, \end{aligned} \quad (4-24)$$

after some algebraic manipulations. The state vector $z \in \mathbb{R}^4$ is defined as $z(e_1, e_2) \triangleq \begin{bmatrix} e_1(t) & e_2(t) \end{bmatrix}^T$. In (4-24), $k \in \mathbb{R}$ is a positive constant, and $\Delta(z) \in \mathbb{R}^2$ is defined as

$$\Delta \triangleq \tilde{W}_1^T \hat{\sigma}' V_1^T y + W_1^T O \left(\tilde{V}_1^T y \right)^2 + \varepsilon(y) + k e_2 + e_1. \quad (4-25)$$

Using (4-20), (4-25), and [69], an upper bound for $\Delta(z)$ can be determined as

$$\|\Delta\| \leq \zeta + \rho(\|z\|) \|z\|, \quad (4-26)$$

where $\rho(\cdot) \in \mathbb{R}$ is a positive, globally invertible, nondecreasing function, and $\zeta \in \mathbb{R}$ is a known positive constant.

4.3 Stability Analysis

Theorem 4.1. *The controller given in (4-15) ensures semi-global asymptotic tracking in the sense that*

$$q_2(t) \rightarrow q_1(t) \quad \text{as } t \rightarrow \infty,$$

provided control gains are selected sufficiently large (see the subsequent stability analysis).

Proof. Let $\mathcal{D} \subset \mathbb{R}^5$ be a domain containing $v(t) = 0$, where $v(t) \in \mathbb{R}^5$ is defined as

$$v(t) \triangleq \begin{bmatrix} z^T(t) & \sqrt{Q(t)} \end{bmatrix}^T, \quad (4-27)$$

and the auxiliary function $Q(t) \in \mathbb{R}$ is defined as

$$Q(t) \triangleq \frac{1}{2} \text{tr} \left(\tilde{V}_1^T \Gamma_{v1}^{-1} \tilde{V}_1 \right) + \frac{1}{2} \text{tr} \left(\tilde{W}_1^T \Gamma_{w1}^{-1} \tilde{W}_1 \right) + \frac{1}{2} \text{tr} \left(\tilde{W}_2^T \Gamma_{w2}^{-1} \tilde{W}_2 \right).$$

Since Γ_{1v} , Γ_{w1} , and Γ_{w2} are constant, symmetric, and positive definite matrices, it is straightforward that $Q(t) \geq 0$.

Let $V(v, t) : \mathcal{D} \times [0, \infty) \rightarrow \mathbb{R}$ be a Lipschitz continuous, regular, positive definite function defined as

$$V \triangleq \frac{1}{2}e_2^T \bar{M} e_2 + \frac{1}{2}e_1^T e_1 + Q, \quad (4-28)$$

which satisfies the following inequalities:

$$U_1(v) \leq V(v, t) \leq U_2(v),$$

where the continuous positive definite functions $U_1(v)$, $U_2(v) \in \mathbb{R}$ are defined as

$$U_1(v) \triangleq \eta_1 \|v\|^2, \quad U_2(v) \triangleq \eta_2 \|v\|^2, \quad (4-29)$$

where $\eta_1, \eta_2 \in \mathbb{R}$ are known positive constants.

The differential equations of the closed loop dynamics given in (4-22) are continuous except in sets $\{v | x = x_t\}$ and $\{v | e_2 = 0\}$. Using Filippov's differential inclusion [70], the existence of solutions can be established for $\dot{v} = f(v)$, where $f(v) \in \mathbb{R}^5$ denotes the right-hand side of the closed-loop error signals. Under Filippov's framework, a generalized Lyapunov stability theory can be used to establish strong stability of the closed-loop error system. The generalized time derivative of (4-28) exists almost everywhere (a.e.), and $\dot{V}(v) \in^{a.e.} \check{V}(v)$ where

$$\check{V} = \bigcap_{\xi \in \partial V} K \left[\begin{array}{ccc} \dot{e}_2 & \dot{e}_1 & \frac{1}{2}Q^{-\frac{1}{2}}\dot{Q} \end{array} \right]^T,$$

where ∂V is the generalized gradient of $V(v)$ [71], $K[\cdot]$ is defined in [72] and [73] as

$$K[f] \triangleq \bigcap_{\delta > 0} \bigcap_{\mu \Upsilon = 0} \bar{c}of(B(x, \delta) - \Upsilon),$$

where $\bigcap_{\mu \Upsilon = 0}$ denotes the intersection of all sets Υ of Lebesgue measure zero, $\bar{c}o$ denotes convex closure, and $B(x, \delta) = \{u \in \mathbb{R}^3 \mid \|u - v\| < \delta\}$. Since $V(v)$ is a Lipschitz continuous regular

function,

$$\begin{aligned}\dot{V} &= \nabla V^T K \begin{bmatrix} \dot{e}_2 & \dot{e}_1 & \frac{1}{2}Q^{-\frac{1}{2}}\dot{Q} \end{bmatrix}^T, \\ &\subset \begin{bmatrix} \bar{M}e_2 & e_1 & 2Q^{\frac{1}{2}} \end{bmatrix}^T K \begin{bmatrix} \dot{e}_2 & \dot{e}_1 & \frac{1}{2}Q^{-\frac{1}{2}}\dot{Q} \end{bmatrix}^T.\end{aligned}\quad (4-30)$$

Using (4-12), (4-20), and (4-22), the expression in (4-30) becomes

$$\dot{V} \subset e_2^T \Delta - \beta \|e_2\| - ke_2^T e_2 - \alpha_1 e_1^T e_1. \quad (4-31)$$

Using (4-26), the expression in (4-31) can be upper bounded as

$$\dot{V} \stackrel{a.e.}{\leq} \rho(\|z\|) \|e_2\| \|z\| - (\beta - \zeta) \|e_2\| - k \|e_2\|^2 - \alpha_1 \|e_1\|^2. \quad (4-32)$$

Let the control gain k in (4-22) be defined as

$$k \triangleq k_1 + k_2, \quad (4-33)$$

where $k_1, k_2 \in \mathbb{R}$ are known positive constants. Using (4-33) and the gain condition

$$\beta > \zeta,$$

the expression in (4-32) can be upper bounded as

$$\dot{V} \stackrel{a.e.}{\leq} - \left(k_1 \|e_2\|^2 - \rho(\|z\|) \|e_2\| \|z\| \right) - k_2 \|e_2\|^2 - \alpha_1 \|e_1\|^2. \quad (4-34)$$

Completing the squares on the term in parentheses in (4-34) yields

$$\dot{V} \stackrel{a.e.}{\leq} \frac{\rho(\|z\|)^2}{4k_1} \|z\|^2 - k_2 \|e_2\|^2 - \alpha_1 \|e_1\|^2. \quad (4-35)$$

The expression in (4-35) can be further upper bounded as

$$\dot{V} \stackrel{a.e.}{\leq} -\lambda \|z\|^2 + \frac{\rho(\|z\|)^2}{4k_1} \|z\|^2, \quad (4-36)$$

where $\lambda = \min\{k_2, \alpha_1\}$ is a known positive constant. Finally, given the gain condition

$$\lambda > \frac{\rho(\|z\|)^2}{4k_1},$$

the expression in (4-36) becomes

$$\dot{V} \stackrel{a.e.}{\leq} -U(v), \quad (4-37)$$

where $U(v) = \mu \|z\|^2$, for some positive constant $\mu \in \mathbb{R}$, is a continuous positive semi-definite function in the domain

$$\mathcal{D} \triangleq \left\{ v \in \mathbb{R}^5 \mid \|v\| \leq \rho^{-1} \left(2\sqrt{\lambda k_1} \right) \right\}.$$

The expressions in (4-28) and (4-37) can be used to show that $V(v, t) \in \mathcal{L}_\infty$; hence, $e_1(t)$, $e_2(t)$, and $Q(t) \in \mathcal{L}_\infty$ in \mathcal{D} . Given that $e_1(t)$, $e_2(t) \in \mathcal{L}_\infty$ in \mathcal{D} , it can be proven that $\dot{e}_1(t) \in \mathcal{L}_\infty$ in \mathcal{D} from (4-12). Since $e_1(t)$, $e_2(t) \in \mathcal{L}_\infty$ in \mathcal{D} , the assumption that $x_d(t)$, $\dot{x}_d(t)$ exist and are bounded can be used to conclude that $x(t)$, $\dot{x}(t) \in \mathcal{L}_\infty$ in \mathcal{D} and $q(t)$, $\dot{q}(t) \in \mathcal{L}_\infty$ in \mathcal{D} using (4-5). Similarly, it can be shown that $\dot{e}_2(t) \in \mathcal{L}_\infty$ in \mathcal{D} . Since $\dot{e}_1(t)$, $\dot{e}_2(t) \in \mathcal{L}_\infty$ in \mathcal{D} , the definitions for $U(v)$ and $z(t)$ can be used to prove that $U(v)$ is uniformly continuous in \mathcal{D} .

Let $\mathcal{S} \subset \mathcal{D}$ denote a set defined as follows:

$$\mathcal{S} \triangleq \left\{ v(t) \in \mathcal{D} \mid U_2(v(t)) < \eta_1 \left(\rho^{-1} \left(2\sqrt{\lambda k_1} \right) \right)^2 \right\}.$$

[74] can now be invoked to state that

$$\|z(t)\|^2 \rightarrow 0 \quad \text{as } t \rightarrow \infty \quad \forall v(0) \in \mathcal{S}. \quad (4-38)$$

Based on the definition of $v(t)$ in (4-27), (4-38) can be used to show that

$$\|e_1(t)\| \rightarrow 0 \quad \text{as } t \rightarrow \infty \quad \forall v(0) \in \mathcal{S}.$$

Using (4-5) and (4-11), the control development ensures that

$$q_2(t) \rightarrow q_1(t) \quad \text{as } t \rightarrow \infty \quad \forall v(0) \in \mathcal{S}.$$

□

Theorem 4.2. *The controller given in (4-15) ensures that the teleoperated system is passive with respect to the scaled user and environmental power.*

Proof. See [53].

□

4.4 Simulation Results

In this section, simulation results are given for two different user input forces to demonstrate the performance of the controller given in (4-15). The master and slave system dynamics are simulated using the following model

$$\begin{aligned} m\ddot{q}_1 + b\dot{q}_1 &= T_1 - F_1, \\ m\ddot{q}_2 + b\dot{q}_2 &= T_2 - f_{needle}(q_2, \dot{q}_2), \end{aligned}$$

where $T_1(t)$ and $T_2(t)$ are introduced in (4-1) and (4-2), $m = 0.152 \text{ kg}$, $b = 1.426 \text{ N} \cdot \text{s} \cdot \text{m}^{-1}$, which correspond to the needle insertion robot described in [75]. The needle insertion force $f_{needle}(q_2, \dot{q}_2)$ is simulated using the design described in Chapter 2, where the needle insertion force is the sum of a stiffness force, a friction force, and a cutting force. As in Chapter 3, the different positions and parameter values are chosen to agree with a direct insertion into the liver. The initial positions are $q_1 = 0 \text{ mm}$ and $q_2 = -20 \text{ mm}$ for $t = 0$. The tissue position is fixed to 200 mm from the origin. The position of the maximally deformed tissue surface before puncture is 216 mm , which means that the needle progresses 16 mm while in contact with the liver before the puncture occurs. The parameters for the desired trajectory introduced in (4-13) are chosen as

$$B_T = 15, \quad K_T = 2.$$

The number of hidden layer neurons for the NN is chosen as $N = 15$, and the NN weight updation gains are selected as

$$\Gamma_{w1} = \Gamma_{w2} = 30I_{16}, \quad \Gamma_{v1} = 30I_5,$$

where $I_p \in \mathbb{R}^{p \times p}$ denotes the identity matrix. For the first simulation, the user input force $F_1(t)$, which corresponds to the force provided by the surgeon on the master robot, is given by a sinusoidal force as

$$F_1 = 15 \sin(1.1t).$$

This simulation does not have a practical meaning because it would mean that the surgeon inserts the needle into a patient, removes it and inserts it again. However, this user trajectory was simulated to demonstrate the performance of the controller under some arbitrary motion. Figure 4-1 shows the master position $q_1(t)$ and the slave position $q_2(t)$. As shown in Figure 4-2, the error between these two position goes to zero as time goes to infinity. The passivity objective, introduced in (4-4), is met when the trajectory of $q_1(t) + q_2(t)$ follows the desired trajectory x_{d2} which can be seen in Figure 4-3 and 4-4.

For the second simulation, the user force $F_1(t)$ is simulated as

$$F_1 = 8.$$

Figures 4-5 and 4-6 show the position tracking between the master robot position $q_1(t)$ and the slave robot position $q_2(t)$. The passivity objective can be seen in Figures 4-7 and 4-8. In Figure 4-9 and 4-10, the needle force f_{needle} is given as a function of time and position of the needle tip, respectively. It can be seen that during the first stage the force between the needle and the tissue is equal to zero because the needle does not touch the tissue yet. Then, the needle force increases to reach a maximum force which is followed by a sudden drop in force as the needle punctures the tissue and now only needs to overcome the friction and cutting forces.

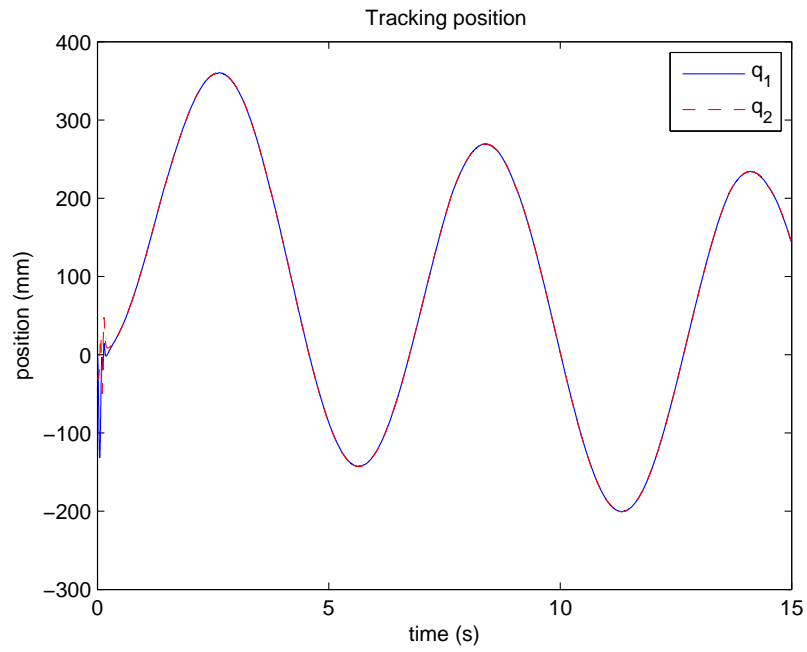


Figure 4-1. Trajectory for master and slave robots for $F_1 = 15 \sin(1.1t)$.

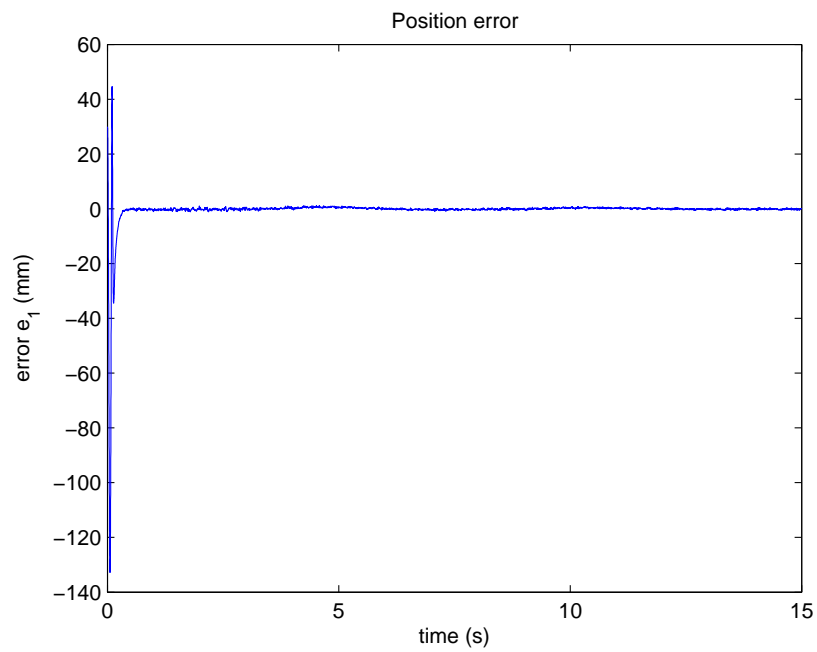


Figure 4-2. Position error between master and slave robot for $F_1 = 15 \sin(1.1t)$.

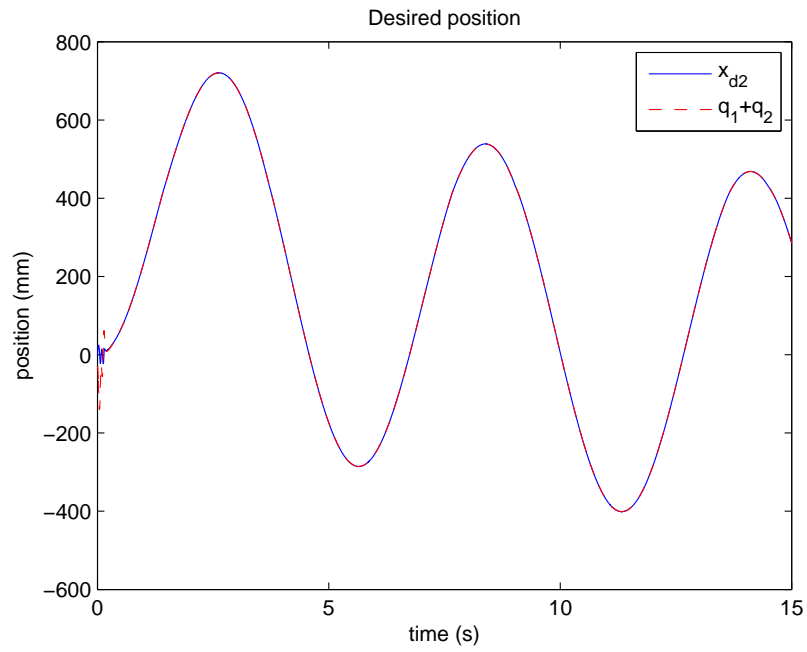


Figure 4-3. Desired trajectory x_{d2} and position of $q_1 + q_2$ for $F_1 = 15 \sin(1.1t)$.

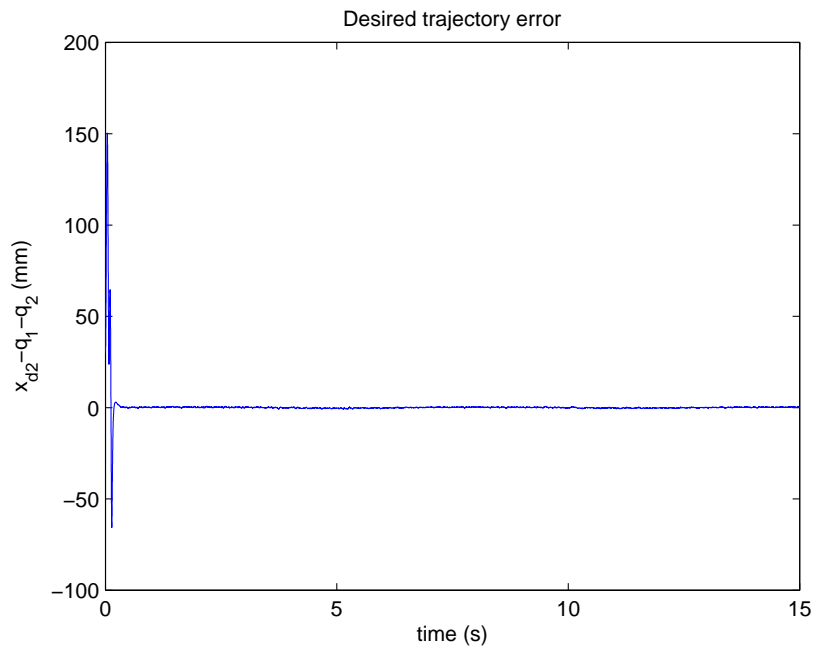


Figure 4-4. Error between the desired trajectory x_{d2} and $q_1 + q_2$ for $F_1 = 15 \sin(1.1t)$.

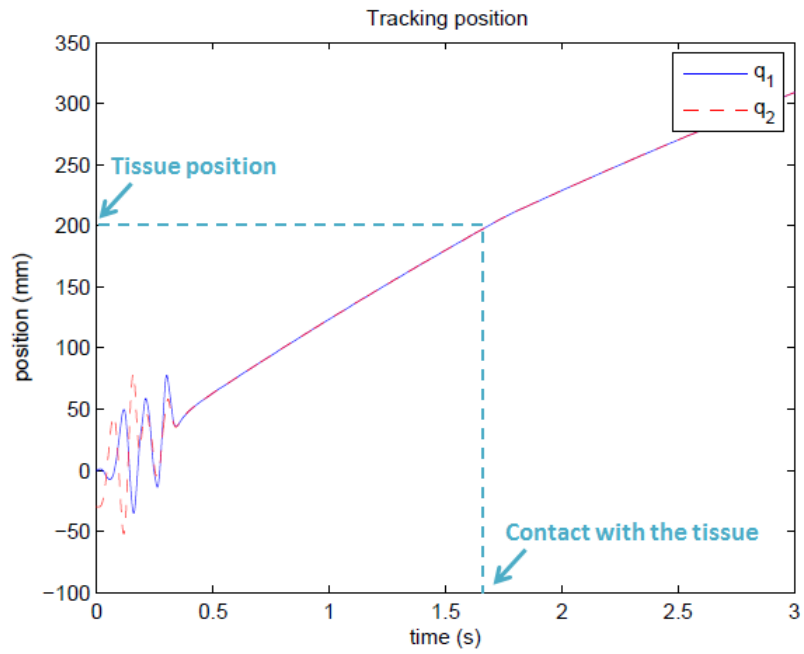


Figure 4-5. Trajectory for master and slave robots for $F_1 = 8$.

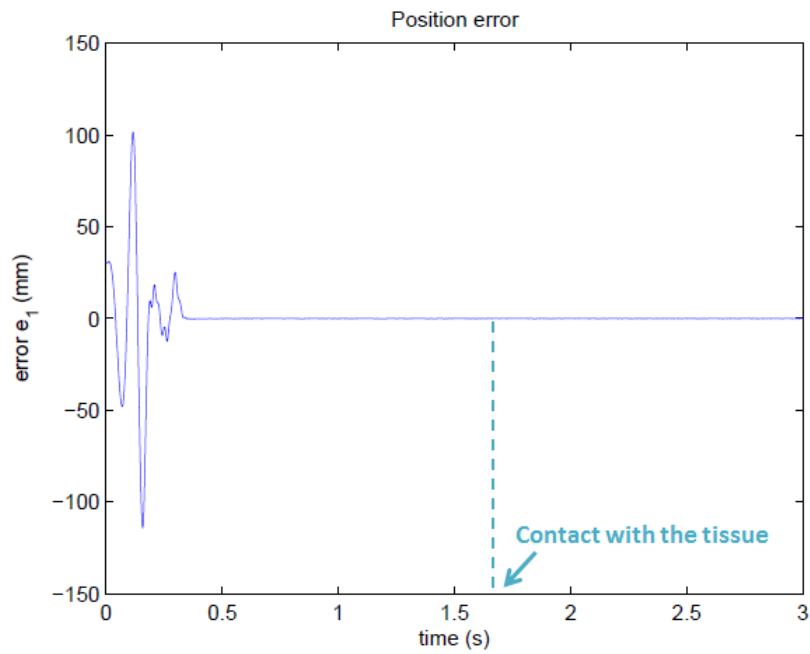


Figure 4-6. Position error between master and slave robot for $F_1 = 8$.

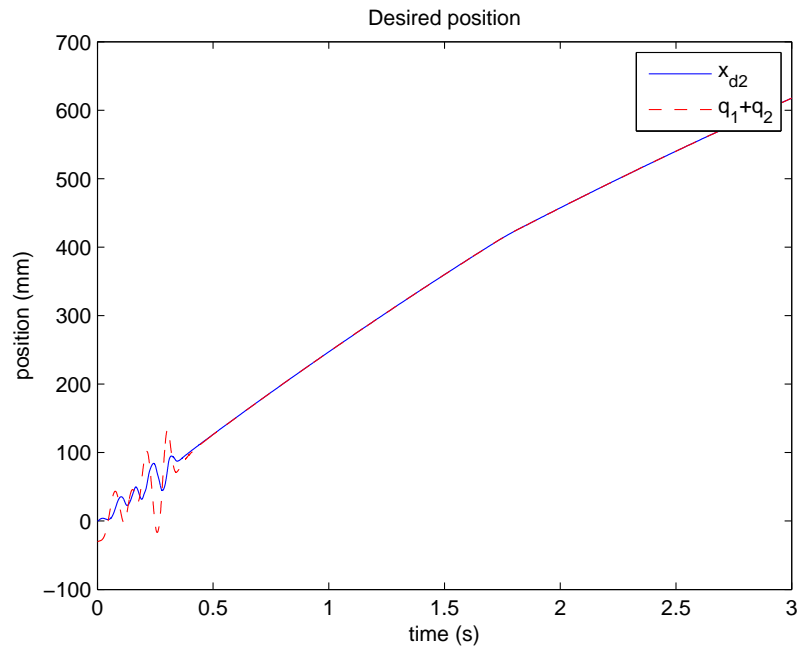


Figure 4-7. Desired trajectory x_{d2} and position of $q_1 + q_2$ for $F_1 = 8$.

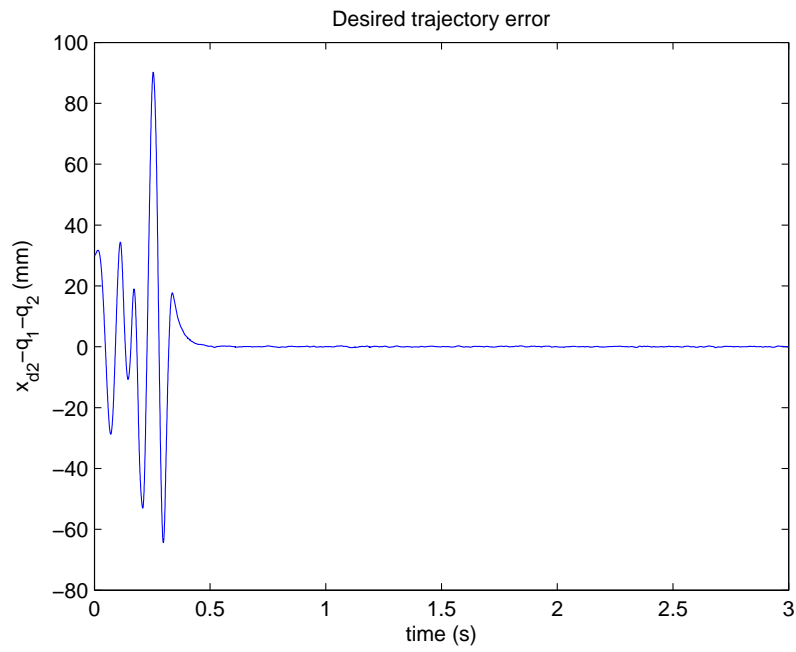


Figure 4-8. Error between the desired trajectory x_{d2} and $q_1 + q_2$ for $F_1 = 8$.

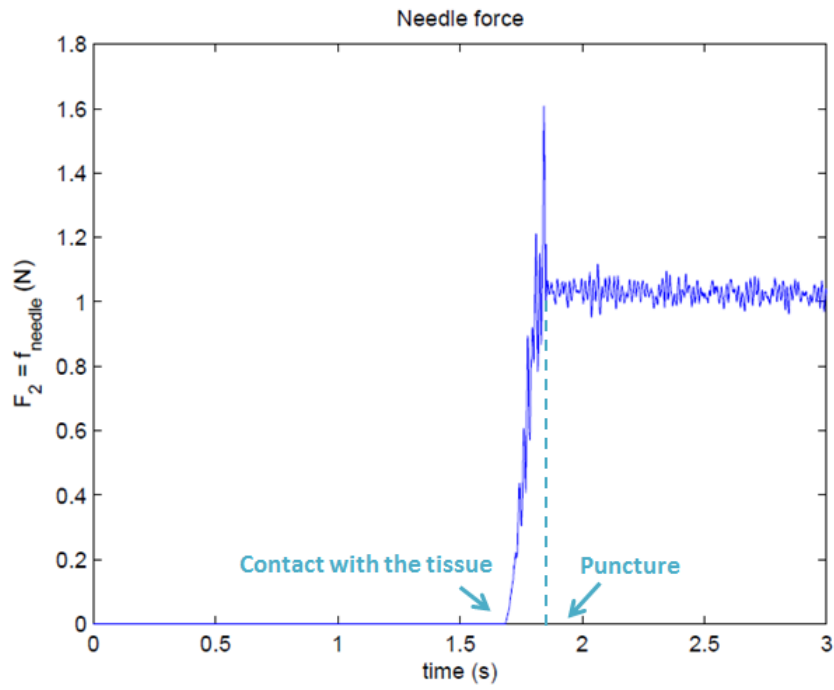


Figure 4-9. Needle force f_{needle} as a function of time for $F_1 = 8$.

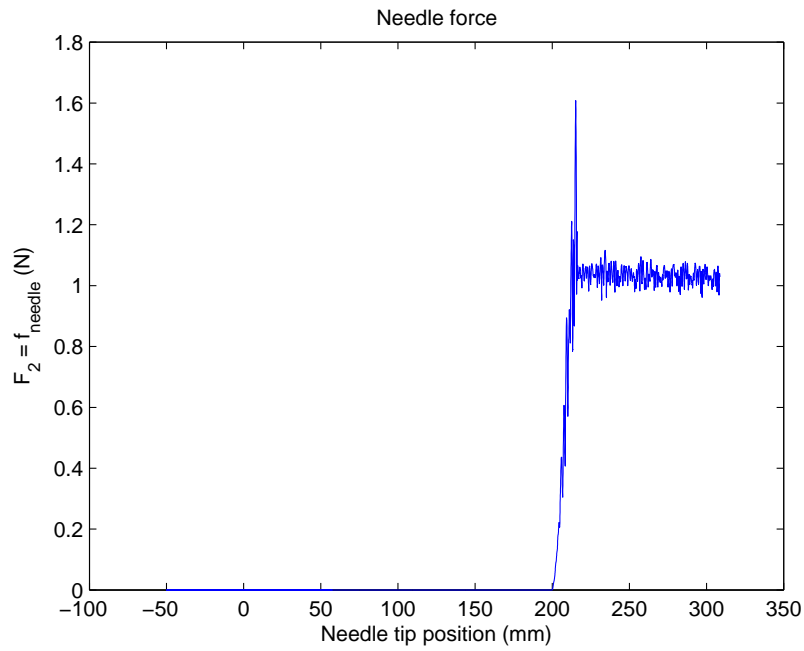


Figure 4-10. Needle force f_{needle} as a function of the needle tip position for $F_1 = 8$.

CHAPTER 5 CONCLUSION

5.1 Summary of Results

In Chapter 2, a discussion on soft tissue deformation is provided. The needle insertion force modeling for viscoelastic tissue is presented as the sum of a Hunt-Crossley stiffness force, a friction force, and a constant cutting force.

In Chapter 3, a one-degree-of-freedom translation robot controller is designed to asymptotically track a desired trajectory going from a non-contact position into a viscoelastic tissue. The needle force is designed considering that the viscoelastic tissue model is the sum of a stiffness force, a friction force, and a cutting force. A sliding mode controller combined with a multi-layer NN is used to ensure asymptotic tracking. A Lyapunov-based stability analysis is provided to prove the semi-global asymptotic tracking. The efficacy of the proposed controller is demonstrated through simulations.

In Chapter 4, a controller is designed to permit a needle insertion slave robot to asymptotically track the position of the master robot going from a non-contact position into a tissue. A globally invertible transformation is defined to show stability and passivity. A Lyapunov-based stability analysis is provided to prove the semi-global asymptotic tracking. Simulation results demonstrate that the position tracking and the passivity objective are met.

Medical robotics research has become an important tool to assist the development of advanced medicine and high precision surgery. Different methods have been studied to insert a needle considering the constraints imposed by the physiological properties of a patient, but also to give haptic feedback, to reduce human errors due to fatigue or hand tremor, and to develop medical simulators to train medical students and surgeons for surgical procedures. Robotic needle insertion can lead to safer and more accurate needle insertions.

5.2 Recommendations for Future Work

In this study, undesired bending of the needle during insertion is not taken into consideration. A bevel tip and tissue deformations can cause the needle to bend during insertion when

using a flexible needle. In clinical practices, a deviation of the needle from the desired path often reduces the effectiveness of the procedures. Experimentally, sensors or imaging devices can be used to acquire data and then control the needle position using rotation and translation.

To improve the controller developed in Chapter 3 and 4, an accurate design for the position of the viscoelastic tissue could be used. The dynamics of the tissue depends on forces from surrounding tissue and organs, and physiological movements as heart beating or breathing. In these chapters, it is only supposed that the position of the tissue depends on time but a specific dynamics is not used. A detailed study of physiological movements could give information about the tissue movement and then it could be applied for the controller development to get a more accurate result. The goal is to be in perfect conformity with the physiological movements but an easier approach could be to employ a mass-spring dynamic.

In Chapter 4, no special care is given for time delay. Time delay affects the performance of dynamic system. Some mechanisms and control strategies can be applied to these systems to compensate for them. For a medical application, there is no real need to compensate for time delay in practice if master and slave robots are close to each other and are directly connected. For a long distance surgery it is fundamental to develop a controller which guarantees stability independent of the delay.

REFERENCES

- [1] J. Rosen, B. Hannaford, M. P. MacFarlane, and M. N. Sinanan, "Force controlled and teleoperated endoscopic grasper for minimally invasive surgery-experimental performance evaluation," *IEEE Trans. Biomed. Eng.*, vol. 46, pp. 1212–1221, 1999.
- [2] O. Piccin, B. L., B. Bayle, M. de Mathelin, and A. Gangi, "A force feedback teleoperated needle insertion device for percutaneous procedures," *Int. J. Robot. Res.*, vol. 28, no. 9, pp. 1154–1168, 2009.
- [3] M. Shoham, M. Burman, E. Zehavi, L. Joskowicz, E. Batkilin, and Y. Kunicher, "Bone-mounted miniature robot for surgical procedures: Concept and clinical applications," *IEEE Trans. Robot. Autom.*, vol. 19, no. 5, pp. 893–901, 2003.
- [4] R. H. Taylor, J. Funda, B. Eldridge, S. Gomory, K. Gruben, D. LaRose, M. Talamini, L. Kavoussi, and J. Anderson, "A telerobotic assistant for laparoscopic surgery," *IEEE Eng. Med. Biol.*, vol. 14, no. 3, pp. 279–288, 1995.
- [5] A. El-Hakim, R. A. Leung, and A. Tewari, "Robotic prostatectomy: a pooled analysis of published literature." *Expert Rev. Anticancer Ther.*, vol. 6, no. 1, pp. 11–20, Jan 2006.
- [6] J. Bauer, B. Lee, D. Stoianovici, J. Bishoff, G. Janetschek, P. Bunyaratavej, W. Kamolpronwjit, S. Ratchanon, S. O'Kelley, J. Cadeddu, S. Micali, F. Micali, M. K. Li, P. Goh, D. Png, and L. Kavoussi, "Remote telesurgical mentoring: feasibility and efficacy," in *System Sciences, 2000. Proceedings of the 33rd Annual Hawaii International Conference on*, jan. 2000, p. 9 pp.
- [7] G. Fichtinger, E. C. Burdette, A. Tanacs, R. Patriciu, D. Mazilu, L. L. Whitcomb, and D. Stoianovici, "Robotically assisted prostate brachytherapy with transrectal ultrasound guidance-phantom experiments," *Brachytherapy*, p. 2006.
- [8] A. Zivanovic and B. Davies, "A robotic system for blood sampling," *IEEE T. Inf. Technol. B.*, vol. 4, pp. 8 –14, 2000.
- [9] S. Dimaio, N. Archip, N. Hata, I.-F. Talos, S. Warfield, A. Majumdar, N. McDannold, K. Hynynen, P. Morrison, W. Wells, D. Kacher, R. Ellis, A. Golby, P. Black, F. Jolesz, and R. Kikinis, "Image-guided neurosurgery at brigham and women's hospital," *IEEE Eng. Med. Biol.*, vol. 25, pp. 67 –73, 2006.
- [10] H. Kataoka, T. Washio, M. Audette, and K. Mizuhara, "A model for relations between needle deflection, force, and thickness on needle penetration," in *Proceedings of the 4th International Conference on Medical Image Computing and Computer-Assisted Intervention*, 2001.
- [11] S. P. DiMaio and S. E. Salcudean, "Needle insertion modeling and simulation," *IEEE Trans. Robot. Autom.*, vol. 19, no. 5, pp. 864–875, Oct. 2003.

- [12] P. N. Brett, A. J. Harrison, and T. A. Thomas, "Schemes for the identification of tissue types and boundaries at the tool point for surgical needles," *IEEE T. Inf. Technol. B.*, vol. 4, no. 1, pp. 30–36, 2000.
- [13] M. P. Ottensmeyer and J. K. Salisbury, "In vivo data acquisition instruments for solid organ mechanical property measurement," in *Int. Conf. Med. Image Comput. Computer-Assisted Interv.*, Oct. 2001, pp. 975–982.
- [14] T. Podder, J. Sherman, E. Messing, D. Rubens, D. Fuller, J. Strang, R. Brasacchio, and Y. Yu, "Needle insertion force estimation model using procedure-specific and patient-specific criteria," in *Engineering in Medicine and Biology Society, 2006. EMBS '06. 28th Annual International Conference of the IEEE*, 2006.
- [15] Y. Kobayashi, T. Sato, and M. Fujie, "Modeling of friction force based on relative velocity between liver tissue and needle for needle insertion simulation," in *Engineering in Medicine and Biology Society, 2009. EMBC 2009. Annual International Conference of the IEEE*, 2009.
- [16] A. Carra and J. Avila-Vilchis, "Multilayer needle insertion modeling for robotic percutaneous therapy," in *Bioinformatics and Biomedical Engineering (iCBBE), 2010 4th International Conference on*, 2010.
- [17] J. Smolen and A. Patriciu, "Model based stabilization of soft tissue targets in needle insertion procedures," in *Engineering in Medicine and Biology Society, 2009. EMBC 2009. Annual International Conference of the IEEE*, 2009.
- [18] K. Hunt and F. Crossley, "Coefficient of restitution interpreted as damping in vibroimpact," *J. Appl. Mech.*, vol. 42, no. 2, pp. 440–445, 1975.
- [19] T. Yamamoto, B. Vagvolgyi, K. Balaji, L. L. Whitcomb, and A. M. Okamura, "Tissue property estimation and graphical display for teleoperated robot-assisted surgery," in *Proc. IEEE Int. Conf. Robot. Autom.*, 2009, pp. 4239–4245.
- [20] L. Barbe, B. Bayle, M. de Mathelin, and A. Gangi, "Needle insertions modeling: Identifiability and limitations," *Biomedical Signal Processing and Control*, vol. 2, no. 3, pp. 191 – 198, 2007.
- [21] R. Alterovitz, K. Goldberg, J. Pouliot, R. Taschereau, and I.-C. Hsu, "Needle insertion and radioactive seed implantation in human tissues: simulation and sensitivity analysis," in *Proc. IEEE Int. Conf. Robot. Autom.*, vol. 2, 2003, pp. 1793–1799.
- [22] N. Diolaiti, C. Melchiorri, and S. Stramigioli, "Contact impedance estimation for robotic systems," *IEEE Trans. Robot. Autom.*, vol. 21, no. 5, pp. 925–935, Oct. 2005.
- [23] A. Haddadi and K. Hashtrudi-Zaad, "A new method for online parameter estimation of hunt-crossley environment dynamic models," in *Proc. IEEE/RSJ Int. Conf. Intell. Robot. Syst.*, 2008, pp. 981–986.

- [24] I. Brouwer, J. Ustin, L. Bentley, A. Sherman, N. Dhruv, and F. Tendick, "Measuring in vivo animal soft tissue properties for haptic modeling in surgical simulation." *Stud Health Technol. Inform.*, vol. 81, pp. 69–74, 2001.
- [25] A. Vilchis, J. Troccaz, P. Cinquin, K. Masuda, and F. Pellissier, "A new robot architecture for tele-echography," *IEEE Trans. Robot. Autom.*, vol. 19, pp. 922 – 926, 2003.
- [26] T. Martinelli, J.-L. Bosson, L. Bressollette, F. Pelissier, E. Boidard, J. Troccaz, and P. Cinquin, "Robot-based tele-echography: clinical evaluation of the ter system in abdominal aortic exploration." *J Ultrasound Med*, vol. 26, pp. 1611–1616, 2007.
- [27] G. Guthart and J. Salisbury, J.K., "The intuitivem telesurgery system: overview and application," in *Robotics and Automation, 2000. Proceedings. ICRA '00. IEEE International Conference on*, 2000.
- [28] R. Rupp and H. J. Gerner, "Neuroprosthetics of the upper extremity—clinical application in spinal cord injury and challenges for the future," *Acta Neurochir. Suppl.*, vol. 97, no. Pt 1, pp. 419–426, 2007.
- [29] K. Hastrudi-Zaad and S. Salcudean, "On the use of local force feedback for transparent teleoperation," in *Robotics and Automation, 1999. Proceedings. 1999 IEEE International Conference on*, 1999.
- [30] H. Kazerooni, T. I. Tsay, and C. L. Moore, "Telefunctioning: An approach to telerobotic manipulations," in *American Control Conference, 1990*, 1990.
- [31] S. Salcudean, "Control for teleoperation and haptic interfaces," in *Control Problems in Robotics and Automation*, ser. Lecture Notes in Control and Information Sciences, B. Siciliano and K. Valavanis, Eds. Springer Berlin / Heidelberg, 1998, vol. 230.
- [32] S. Salcudean, K. Hashtrudi-Zaad, S. Tafazoli, S. DiMaio, and C. Reboulet, "Bilateral matched impedance teleoperation with application to excavator control," *IEEE Contr. Syst.*, vol. 19, pp. 29 –37, 1999.
- [33] Y. Yokokohji and T. Yoshikawa, "Bilateral control of master-slave manipulators for ideal kinesthetic coupling-formulation and experiment," in *Robotics and Automation, 1992. Proceedings., 1992 IEEE International Conference on*, 1992.
- [34] R. Adams and B. Hannaford, "Stable haptic interaction with virtual environments," *IEEE Trans. Robot. Autom.*, vol. 15, pp. 465 –474, 1999.
- [35] J. Colgate, "Robust impedance shaping telemanipulation," *IEEE Trans. Robot. Autom.*, vol. 9, pp. 374 –384, 1993.
- [36] R. Anderson and M. Spong, "Bilateral control of teleoperators with time delay," *IEEE Trans. Autom. Control*, vol. 34, no. 5, pp. 494–501, May 1989.

- [37] K. Hashtrudi-Zaad and S. Salcudean, "Adaptive transparent impedance reflecting teleoperation," in *Robotics and Automation, 1996. Proceedings., 1996 IEEE International Conference on*, 1996.
- [38] H.-K. Lee, M. H. Shin, and M. J. Chung, "Adaptive controller of master-slave systems for transparent teleoperation," in *Advanced Robotics, 1997. ICAR '97. Proceedings., 8th International Conference on*, 1997.
- [39] J.-H. Ryu and D.-S. Kwon, "A novel adaptive bilateral control scheme using similar closed-loop dynamic characteristics of master/slave manipulators," *J. Robot. Syst.*, vol. 18, pp. 533–543, 2001.
- [40] Y. Yokokohji, T. Imaida, and T. Yoshikawa, "Bilateral control with energy balance monitoring under time-varying communication delay," in *Robotics and Automation, 2000. Proceedings. ICRA '00. IEEE International Conference on*, 2000.
- [41] D. Lee and P. Li, "Passive tool dynamics rendering for nonlinear bilateral teleoperated manipulators," in *Robotics and Automation, 2002. Proceedings. ICRA '02. IEEE International Conference on*, 2002.
- [42] B. Miller, J. Colgate, and R. Freeman, "Guaranteed stability of haptic systems with nonlinear virtual environments," *IEEE Trans. Robot. Autom.*, vol. 16, pp. 712–719, 2000.
- [43] G. Niemeyer and J.-J. Slotine, "Stable adaptive teleoperation," *IEEE J. Oceanic. Eng.*, vol. 16, pp. 152–162, 1991.
- [44] D. Lee and P. Y. Li, "Passive coordination control to nonlinear bilateral teleoperated manipulators," in *In 2002 IEEE International Conf. on Robotics and Automation*, 2002.
- [45] B. Hannaford, "A design framework for teleoperators with kinesthetic feedback," *IEEE Trans. Robot. Autom.*, vol. 5, pp. 426–434, 1989.
- [46] H.-K. Lee, M. H. Shin, and M. J. Chung, "Adaptive controller of master-slave systems for transparent teleoperation," in *Advanced Robotics, 1997. ICAR '97. Proceedings., 8th International Conference on*, 1997.
- [47] N. Chopra and M. Spong, "Adaptive coordination control of bilateral teleoperators with time delay," in *Decision and Control, 2004. CDC. 43rd IEEE Conference on*, . 2004.
- [48] A. M. Okamura, C. Simone, and M. D. O'Leary, "Force modeling for needle insertion into soft tissue," *IEEE Trans. Biomed. Eng.*, vol. 51, no. 10, pp. 1707–1716, Oct. 2004.
- [49] C. Makkar, G. Hu, W. G. Sawyer, and W. E. Dixon, "Lyapunov-based tracking control in the presence of uncertain nonlinear parameterizable friction," *IEEE Trans. Automat. Control*, vol. 52, pp. 1988–1994, 2007.
- [50] S. Bhasin, P. Patre, Z. Kan, and W. E. Dixon, "Control of a robot interacting with an uncertain viscoelastic environment with adjustable force bounds," in *Proc. Am. Control Conf.*, Baltimore, MD, 2010, pp. 5242–5247.

- [51] S. Bhasin, K. Dupree, P. Patre, and W. E. Dixon, "Neural network control of a robot interacting with an uncertain hunt-crossley viscoelastic environment," in *Proc. ASME Dyn. Syst. Control Conf.*, Ann Arbor, Michigan, September 2008.
- [52] S. Bhasin, K. Dupree, Z. D. Wilcox, and W. E. Dixon, "Adaptive control of a robotic system undergoing a non-contact to contact transition with a viscoelastic environment," in *Proc. Am. Control Conf.*, St. Louis, Missouri, June 2009, pp. 3506–3511.
- [53] M. McIntyre, W. E. Dixon, D. Dawson, and E. Tatlicioglu, "Passive coordination of nonlinear bilateral teleoperated manipulators," in *Proc. IEEE/ASME Int. Conf. Adv. Intell. Mechatron.*, Monterey, CA, July 2005, pp. 1287–1292.
- [54] T. Hu and J. Desai, "Soft-tissue material properties under large deformation: strain rate effect," in *Engineering in Medicine and Biology Society, 2004. IEMBS '04. 26th Annual International Conference of the IEEE*, 2004.
- [55] M. Palmeri, A. Sharma, R. Bouchard, R. Nightingale, and K. Nightingale, "A finite-element method model of soft tissue response to impulsive acoustic radiation force," *IEEE Trans. Ultrason., Ferroelec., and Freq. Control*, vol. 52, pp. 1699–1712, 2005.
- [56] H. Tanoue, Y. Hagiwara, K. Kobayashi, and Y. Saijo, "Ultrasonic tissue characterization of prostate biopsy tissues by ultrasound speed microscope," in *Engineering in Medicine and Biology Society, EMBC, 2011 Annual International Conference of the IEEE*, 2011.
- [57] G. Boyer, H. Zahouani, A. Le Bot, and L. Laquieze, "In vivo characterization of viscoelastic properties of human skin using dynamic micro-indentation," in *Engineering in Medicine and Biology Society, 2007. EMBS 2007. 29th Annual International Conference of the IEEE*, 2007.
- [58] W. F. Larrabee, "A finite element model of skin deformation. i. biomechanics of skin and soft tissue: A review," *The Laryngoscope*, vol. 96, pp. 399–405, 1986.
- [59] R. Minns, P. Soden, and D. Jackson, "The role of the fibrous components and ground substance in the mechanical properties of biological tissues: A preliminary investigation," *J. Biomech.*, vol. 6, pp. 153 – 165, 1973.
- [60] S. Vesentini, A. Redaelli, and F. Montecvecchi, "A two-dimensional recruitment model for the skin," in *Molecular, Cellular and Tissue Engineering, 2002. Proceedings of the IEEE-EMBS Special Topic Conference on*, 2002.
- [61] Y. C. Fung, *Biomechanics: Mechanical Properties of Living Tissue*, 2nd ed. New York: Springer-Verlag, 1993.
- [62] C. Makkar, W. E. Dixon, W. G. Sawyer, and G.H, "A new continuously differentiable friction model for control systems design," in *Proc. IEEE/ASME Int. Conf. Adv. Intell. Mechatron.*, Monterey, CA, July 2005, pp. 600–605.
- [63] J. Hollerbach and K. Suh, "Redundancy resolution of manipulators through torque optimization," *IEEE J. Robot. Autom.*, vol. 3, pp. 308–316, 1987.

- [64] W. E. Dixon, M. S. de Queiroz, D. M. Dawson, and F. Zhang, "Tracking control of robot manipulators with bounded torque inputs," *Robotica*, vol. 17, pp. 121–129, 1999.
- [65] L. Barbe, B. Bayle, M. De Mathelin, and A. Gangi, "In vivo model estimation and haptic characterization of needle insertions," *Int. J. Rob. Res.*, vol. 26, pp. 1283–1301, 2007.
- [66] F. L. Lewis, R. Selmic, and J. Campos, *Neuro-Fuzzy Control of Industrial Systems with Actuator Nonlinearities*. Philadelphia, PA, USA: Society for Industrial and Applied Mathematics, 2002.
- [67] M. Krstic, P. V. Kokotovic, and I. Kanellakopoulos, *Nonlinear and Adaptive Control Design*. John Wiley & Sons, 1995.
- [68] W. E. Dixon, A. Behal, D. M. Dawson, and S. Nagarkatti, *Nonlinear Control of Engineering Systems: A Lyapunov-Based Approach*. Birkhäuser: Boston, 2003.
- [69] F. Lewis, A. Yesildirek, and K. Liu, "Multilayer neural net robot controller: structure and stability proofs," *IEEE Trans. Neural Networks*, vol. 7, no. 2, pp. 388–399, 1996.
- [70] A. Filippov, "Differential equations with discontinuous right-hand side," *Am. Math. Soc. Transl.*, vol. 42 no. 2, pp. 199–231, 1964.
- [71] F. H. Clarke, *Optimization and nonsmooth analysis*. SIAM, 1990.
- [72] D. Shevitz and B. Paden, "Lyapunov stability theory of nonsmooth systems," *IEEE Trans. Autom. Control*, vol. 39 no. 9, pp. 1910–1914, 1994.
- [73] B. Paden and S. Sastry, "A calculus for computing Filippov's differential inclusion with application to the variable structure control of robot manipulators," *IEEE Trans. Circuits Syst.*, vol. 34 no. 1, pp. 73–82, 1987.
- [74] H. K. Khalil, *Nonlinear Systems*, 3rd ed. Prentice Hall, 2002.
- [75] M. Joinie-Maurin, B. Bayle, and J. Gangloff, "Force feedback teleoperation with periodical disturbance compensation," in *Robotics and Automation (ICRA), 2011 IEEE International Conference on*, 2011.
- [76] J. C. Willems, "Dissipative dynamical systems part i: General theory," *Archive for Rational Mechanics and Analysis*, vol. 45, pp. 321–351, 1972.

BIOGRAPHICAL SKETCH

Céline Laplassotte was born in Wissembourg, France in 1989. In 2009, she entered at Télécom Physique Strasbourg, France. The year after, she pursued her study with the Master Imagerie Robotique et Ingénierie pour le Vivant (Imaging, Robotics and Engineering for Surgery) at the University of Strasbourg. Her interests lie in the field of nonlinear control, biomedical engineering and robotics.

Thanks to the Atlantis program, Céline pursued a dual Master of Science degree between the University of Strasbourg and the Nonlinear Controls and Robotics group in the Department of Mechanical and Aerospace Engineering at the University of Florida, under the supervision of Dr. Warren E. Dixon. During her laboratory time, she had the opportunity to work on robotic needle insertion.